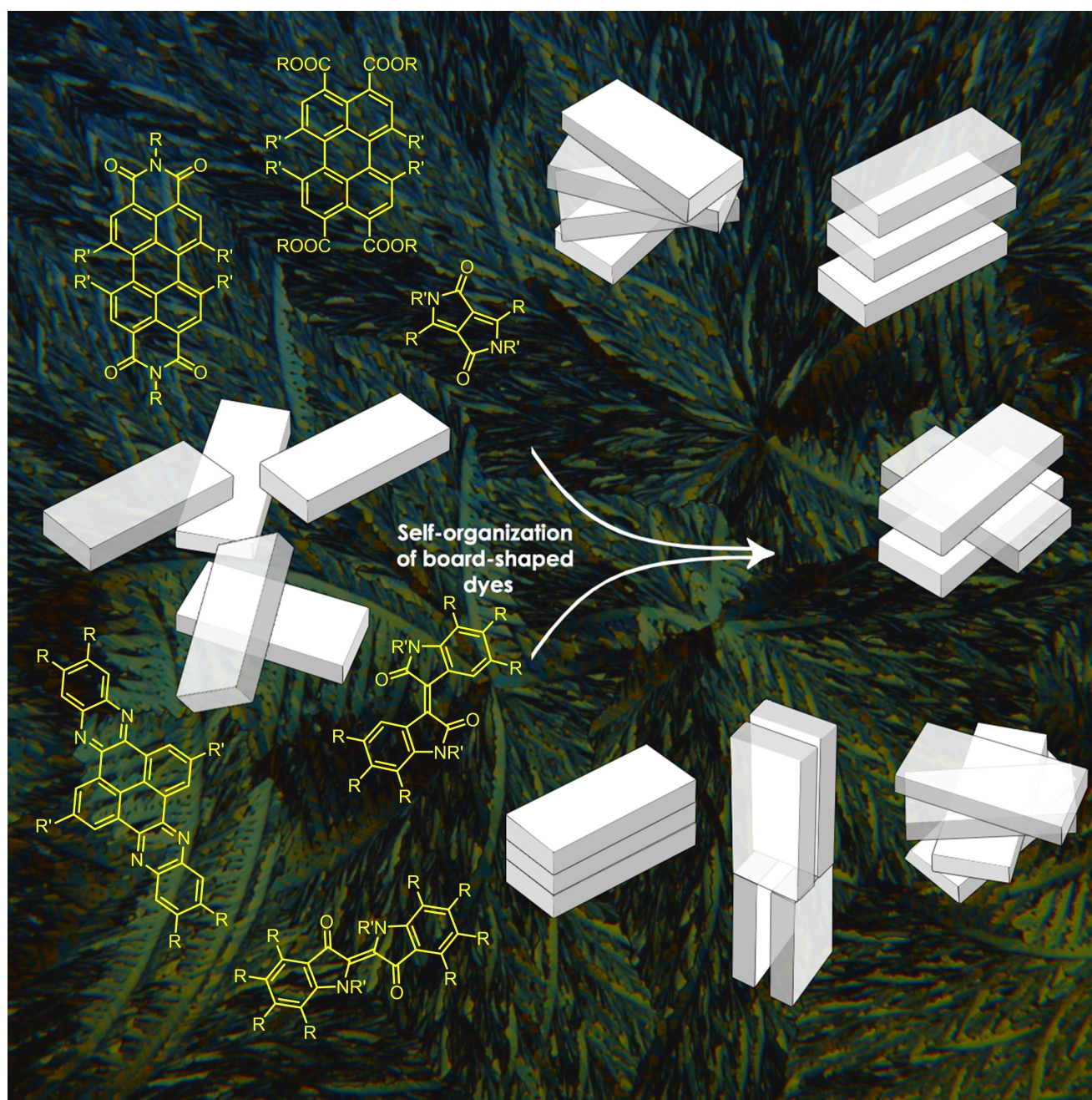


Columnar Mesomorphism of Board-Shaped Perylene, Diketopyrrolopyrrole, Isoindigo, Indigo, and Quinoxalino-Phenanthrophenazine Dyes

S. Holger Eichhorn,^{*,[a]} A. O. El-Ballouli,^[b, c] Adam Cassar,^[a] and Bilal R. Kaafarani^{*,[d]}



The properties of organic dyes depend as much on their intermolecular interactions as on their molecular structure. While it is generally predictable what supramolecular structure would be ideal for a specific application, the generation of specific supramolecular structures by molecular design and suitable processing methods remains to be a challenge. A versatile approach to different supramolecular structures has been the application of mesomorphism in conjunction with alignment techniques and self-assembly at interfaces. Reviewed

here is the columnar mesomorphism of board-shaped dyes perylene, indigo, isoindigo, diketopyrrolopyrrole, and quinoxalino-phenanthrophenazine. They generate a larger number of different supramolecular structures than conventional disc-shaped (discotic) mesogens because of their non-circular shape and directional intermolecular interactions. The mesomorphism of all but the perylene derivatives is systematically and comprehensively covered for the first time.

1. Introduction

Optical and electronic properties of organic dyes and pigments in the solid state crucially depend on not only their molecular structure but also their 3-dimensional molecular packing and intermolecular interactions.^[1,2] Their packing or supramolecular structures are dictated by their crystalline,^[3–5] amorphous,^[6] solid or meso-phases^[7] (liquid crystalline phases, and plastic and condensation crystals). For applications in organic electronics, mesophases have the advantage of combining a sufficiently high degree of packing order with the potential formation of large monodomains of uniform alignment.^[8,9] On the other hand, higher molecular dynamics in mesophases may reduce charge transport and negatively affect other electronic properties in comparison to an ideally structured crystalline phase.^[10,11]

Mesophase formation and structure are dictated by shape-anisotropy, microphase segregation and packing volumes of segregated parts, and, to a lesser degree, by directional intermolecular interactions.^[12,13] The two main anisotropic shapes for mesogens are either rod-shaped (calamitic) for the formation of nematic and smectic (lamellar) mesophases, or disc-shaped (discotic) for the formation of nematic and columnar mesophases (Figure 1).

Ideal calamitic molecules have Length to Breadth to Width values of $L \gg B \geq W$ and ideal discotic molecules have values of $L = B \gg W$. Deviation from these two fundamental shapes has been a fruitful exercise in the design of new mesophase structures and has led to a better understanding of the fundamental forces that govern self-organization.^[14,15] Board-shaped compounds, also referred to as lath-shaped or sanidic molecules,^[16,17] combine the shape anisotropy of rod- and disc-

shaped structures, which makes them multipotent building blocks for nematic, lamellar (smectic) and columnar mesophases. They have been applied widely in liquid crystal science (Figure 1).

Indeed, board-shaped compounds have long been regarded as the most promising building blocks for the elusive thermotropic biaxial nematic mesophase since their shape anisotropy may prevent free rotation about the long axis of the molecules. In fact, specific aspect ratios $L:B:W$ of 15:5:3 (Luckhurst)^[18] and 10:3.16:1 (Straley)^[19] for length to breadth to width, respectively, have been proposed based on experimental and theoretical studies to be ideal for the formation of this still elusive mesophase.^[20]

Smaller overall length to breadth ratios (core and side-chains) than three ($L:B < 3$) generally promote columnar over nematic and smectic mesomorphism as long as the flexible side-chains are adequately positioned and have sufficient packing volume for generating a side-chain continuum around segregating stacking cores (columnar stacks). The width is much smaller than the breadth ($B \gg W$) and typically does not vary much between different aromatic cores and side-chains, which is why it is omitted in the following.

Reviewed here is the columnar mesomorphism of five board-shaped dyes perylene (PBI and PTE),^[21–24] indigo (IND),^[25,26] isoindigo (IIND),^[25,27–29] diketopyrrolopyrrole (DPP),^[28,30–35] and quinoxalino-phenanthrophenazine (QPP)^[36,37] (Figure 2). They were selected because of their significant industrial importance (perylene, IND, and DPP) and their specific mesomorphism has not been reviewed except for perylene. A ranking of the core structures by in-plane aspect ratios ($L:B$)

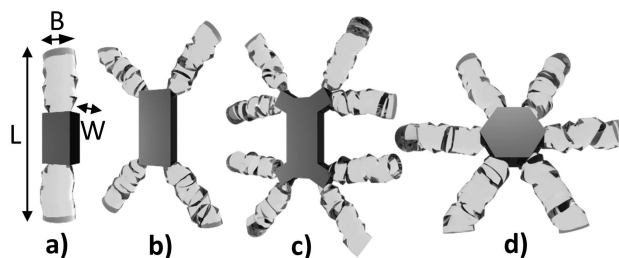


Figure 1. Cartoons of a) typical rod-shaped and d) disc-shaped molecular structures with characteristic Length to Breadth to Width ($L:B:W$) ratios of 15:2.5:1 and 20:20:1, respectively. Structures b) and c) illustrate two board-shaped structures with different $L:B:W$ values of 23:11:1 and 27:20:1, respectively. The more rigid core structures and amorphous aliphatic side-chains are illustrated as dark boxes and glass-like segments, respectively, of realistic relative dimensions.

[a] Prof. Dr. S. H. Eichhorn, A. Cassar
Department of Chemistry and Biochemistry
University of Windsor
401 Sunset Ave, Windsor, ON, N9B 3P4 (Canada)
E-mail: eichhorn@uwindsor.ca

[b] Dr. A. O. El-Ballouli
College of Science and Health Professions
King Saud bin Abdulaziz University for Health Sciences
Riyadh 11481 (Kingdom of Saudi Arabia)

[c] Dr. A. O. El-Ballouli
King Abdullah International Medical Research Center
Riyadh 11426 (Kingdom of Saudi Arabia)

[d] Prof. Dr. B. R. Kaafarani
Department of Chemistry
American University of Beirut
Beirut 1107-2020 (Lebanon)
E-mail: bilal.kaafarani@aub.edu.lb

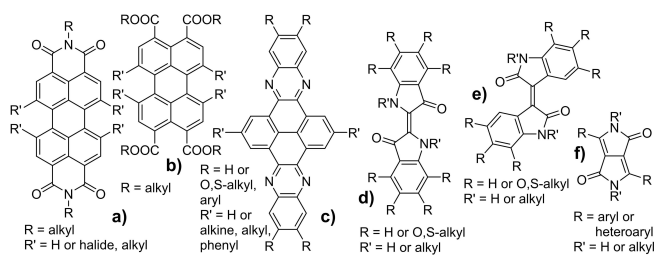


Figure 2. Board-shaped dyes a) perylene bisimide (PBI), b) perylene tetraesters (PTE), c) quinoxalino[2,3-g]phenanthro[9,10-b]quinoxaline (QPP), d) indigo (In), e) isoindigo (IIn), and f) diketopyrrolopyrrole (DPP). "Alkyl" includes linear and branched chains as well as oligoethers and otherwise functionalized alkyl chains.

gives the following order: 1.47 for perylene tetracarboxylic ester (PTE), 1.66 for perylene tetracarboxylic bisimide (PBI), 1.77 for QPP, 1.80 for isoindigo, 2.04 for dithiophene DPP, and 2.37 for indigo. Structures with a smaller aspect ratio are more easily converted into columnar liquid crystals, which may be one reason for why PBI has been the most widely studied core structure of those five. Of course, the aspect ratios of cores and entire molecules can be widely altered by the attachment of substituents and another reason for the much larger body of work on the columnar mesomorphism of perylene derivatives^[38–40] when compared to the small number of columnar mesomorphic indigo, isoindigo, diketopyrrolopyrrole, and quinoxalino[2,3-g]phenanthro[9,10-b]quinoxaline derivatives may be restrictions in synthetically achievable substitution patterns for the latter. In addition, the lactam containing cores have a very high propensity for solidification and crystallization.

A potential advantage of board-shaped over discotic columnar mesomorphic dyes is the preferential formation of higher ordered columnar packing structures that are more difficult to achieve with conventional disc-shaped molecules. Most disc-shaped molecules arrange into uniaxial hexagonal columnar mesophases with electronic properties of *H*-aggregates (face-to-face packing) and display a fast rotation over their stacking axis.^[41,42] So, the relative orientation of stacking molecules is ill-defined, although strong π - π stacking interactions between conventional discotic molecules have induced more defined relative orientations and tilt in columnar π - π stacks.^[43]

In contrast, the in-plane shape anisotropy of board-shaped molecules conduces to columnar mesophases of lower symmetry and higher order that may display properties of *J*-aggregates (slipped packing) and reduced rotational dynamics.^[44] As illustrated in Figure 3, board-shaped molecules are more likely to arrange into tilted, helical, and other columnar stacks with correlation of intracolumnar orientation. This often leads to better defined intermolecular interactions and allows for the adjustment of optoelectronic properties, such as fluorescence and charge transport.^[36,45,46]

Several unusual columnar mesophase structures have been reported for some of these board-shaped dyes and it is our intention to specifically highlight rare supramolecular structures and their underlying molecular structures. Concepts such as shape-anisotropy (aspect ratios), nanosegregation, and relative packing volumes were applied qualitatively to reason the formation of different types of columnar mesophase based on molecular design.^[12]

Not covered in this review are liquid crystalline polymers that contain these dye cores as one of several components and



S. Holger Eichhorn has been trained in dye chemistry and photopolymerization during his Ph.D. at the University of Bremen (D. Wöhrlé). He became proficient in the synthesis and characterization of liquid crystalline compounds as a postdoctoral researcher during stays at Exeter University (D. Bruce), Leeds University/SOMS Centre (R. Bushby, N. Boden) and the Massachusetts Institute of Technology (T. Swager). Since he started his independent career at the University of Windsor in 2001, his group has contributed a wide range of different mesomorphic, amphiphilic, and polymerizable dyes.



Ala'a El-Ballouli holds a M.Sc. in Chemistry from the American University of Beirut (AUB), Lebanon (2011); and a Ph.D. in Material Science and Engineering from King Abdullah University of Science and Technology (KAUST), KSA (2016). She is currently an Assistant Professor of Chemistry at King Saud bin Abdulaziz University for Health Sciences (KSAU-HS), KSA where she focuses on studying organic materials and inorganic nanoparticles for optoelectronic applications.



Adam Cassar worked on liquid crystalline DPP and isoindigo derivatives as an undergraduate research student under the supervision of Eichhorn and Taing (Ph.D. student at the time) at the University of Windsor. He started his M.Sc. in the Eichhorn group in 2019 to continue his work on mesomorphic DPP derivatives with a focus on fluorescent materials. Adam is an avid traveller and presently searching for a Ph.D. position outside North America.



Bilal R. Kaafarani is an Organic and Materials chemist. He received his Ph.D. in Photochemical Sciences from Bowling Green State University in 2002. After Postdoctoral work at the University of Arizona and the Georgia Institute of Technology, he joined the department of Chemistry at the American University of Beirut as Assistant Professor of Chemistry in September 2004. He was promoted to Associate Professor in 2010 and subsequently to Full Professor in 2016. Kaafarani's research area spans the field of organic electronics and sensors. Kaafarani is an advocate of interactive learning, experiential learning and transformative education.

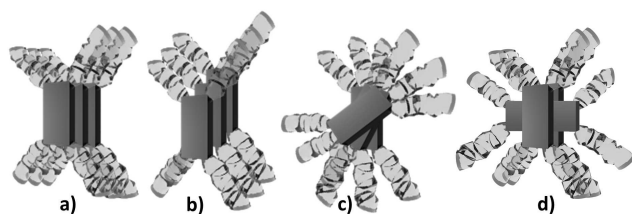


Figure 3. Idealized stacking structures of board-shaped dyes in columnar mesophases. The rigid core and amorphous aliphatic side-chains are illustrated as dark boxes and glass-like segments, respectively, and have realistic relative dimensions. Structure a) is the least likely for board-shaped dyes because of unfavourable space filling by the side-chains and often non-ideal stacking interactions between cores. More favourable for columnar mesophases of board-shaped compounds are packing structures that b) involve stacks with laterally shifted cores and/or columnar stacks of cores that are rotated about their stacking axis by specific values to give, for example, c) helical columnar mesophase and d) columnar mesophase with orthogonal stacking of the long axis of the cores.

the use of these dyes as additives to liquid crystal matrices for the generation of anisotropic optical materials. Also, outside the scope of this review are dye derivatives that self-assemble on surfaces and at interfaces. However, references to some of these studies are provided where deemed valuable.

2. Mesomorphic Perylene Dyes

A comprehensive review of the large body of work on mesomorphic derivatives of perylene has recently been provided elsewhere.^[40] The intention here is to highlight some detailed studies on structure-property relations and unusual modes of self-organization that have been reported for perylene tetracarboxylic bisimides (PBIs) and its much less studied tetraesters (PTEs).

2.1. Perylene Tetracarboxylic Bisimide (PBI)

Perylene tetracarboxylic bisimide (PBI), also recognized as perylene-3,4,9,10-tetracarboxylic diimide (PDI), is a planar chromophore that is well-known for its n-type (electron-accepting) characteristics and high thermal, chemical, and photostability.^[38,47–49] In addition to its desirable physical properties, the chromophore permits various chemical functionalizations at the (i) bay-regions (1,6,7,12-positions), (ii) ortho-regions (2,5,8,11-positions), and (iii) imide-positions (Figure 4), thus

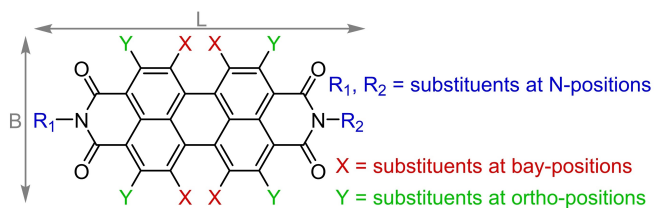


Figure 4. General substitution pattern for PBIs and their length (L) to breadth (B) measurement including R, X, and Y groups.

offering structural diversity for applications in various research fields such as coatings, biochemistry, supramolecular chemistry, organic electronics, and sensors.^[9,50–56]

All PBIs show strong absorption in the visible spectral region with absorption maxima between 510 and 570 nm, depending on the core substituents, along with high fluorescence quantum yields.^[38]

In addition, changes in the structural growth (or self-assembly) of PBI building blocks often result in drastic changes in their absorption and fluorescence properties. The influence of the packing arrangement on the optical properties of PBIs is apparent through their solid-state coloristic properties that vary between red, maroon, and even black. This was achieved by changing imide substituents that do not impact the molecular chromophore but their intermolecular interactions and packing structures.^[38,57]

In solution, PBIs often form concentration-dependent aggregates based on the solvents' polarity and temperature. Fluorescence quantum yields near-unity have been reported for many derivatives in dilute solutions that often decrease with increasing concentration and aggregation.^[58–62] Aggregation-caused quenching (ACQ) also lowers the emission of many PBIs in crystalline and solid states.^[63,64]

Liquid crystallinity has been particularly attractive for controlling the supramolecular self-assembly of PBIs in condensed phases^[40] even though the formation of specific aggregates and crystal structures has also been broadly studied in the solid-state and in solution.^[38,65] Their strong intermolecular π - π stacking forces are advantageous for the induction of mesomorphism if properly balanced by flexible side-chains that lower melting temperatures and increase solubility. A number of PBI derivatives with *n*-alkyl^[66,67] and simple cycloalkyl,^[63] and aromatic^[57] substituents at their imide positions form crystalline phases of too high melting temperatures for mesomorphism to be observable or practical.

However, attachment of appropriate flexible side-chains to the two N-terminals has been shown to be sufficient for the induction of mesomorphism at temperatures well below 200 °C. Substitution of the bay-positions (see Figure 4) has been less frequently used for adjusting self-organization mainly because the synthesis of these derivatives is less straightforward, and we are not aware of mesomorphic PBIs with substituents in the ortho-positions. Substituents in the bay-positions are especially effective in altering mesomorphism because they reduce the L:B (in-plane) aspect ratio and often cause twisting of the otherwise planar PBI core. Strong intermolecular interactions, such as hydrogen bonding, charge transfer, metal coordination, and ionic interactions have been widely utilized for promoting and directing the self-assembly of PBIs,^[38] but rather little for the support of mesomorphism.^[40]

N-substituted PBIs with single and swallow tail side-chains constitute the first studied mesomorphic PBI derivatives and have some of the largest L:B aspect ratios (Figure 5). Gregg and co-workers were the first to report liquid-crystalline properties for PBIs in 1997.^[68–71] Their compounds contained propoxy and ethylphenyl linking groups with single and branched oligo (ethyleneoxy) chains at the imide N-positions. Two examples

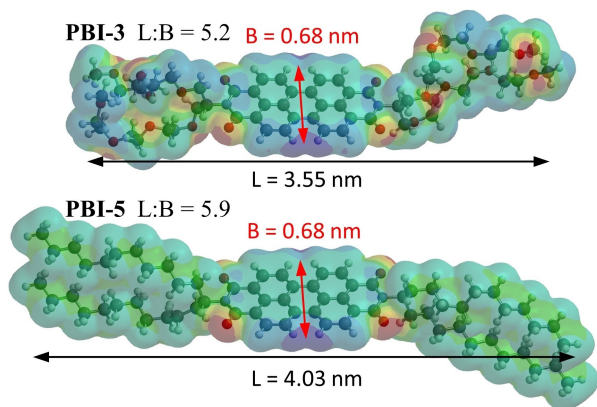


Figure 5. Electrostatic potential maps projected onto density surfaces generated by semiempirical PM6 calculations (Spartan) for **PBI-3** and **PBI-5** in the gas phase. In-plane aspect ratios are calculated based on estimated molecular lengths for side-chains in amorphous states and the breadth of the PBI core.

are **PBI-1** and **-2** in Figure 6 and Table 1. Unfortunately, no X-ray diffraction data were provided for any of the compounds to verify the columnar mesomorphism and **PBI-1** crystallized within 24 hours as spin-coated thin film, which indicates that the observed mesophase is not thermodynamically stable at room temperature.

In general, oligo(ethyleneoxy) side-chains are much more effective in inducing mesomorphism in N-substituted PBIs than the otherwise more regularly used alkyl chains. This is mainly

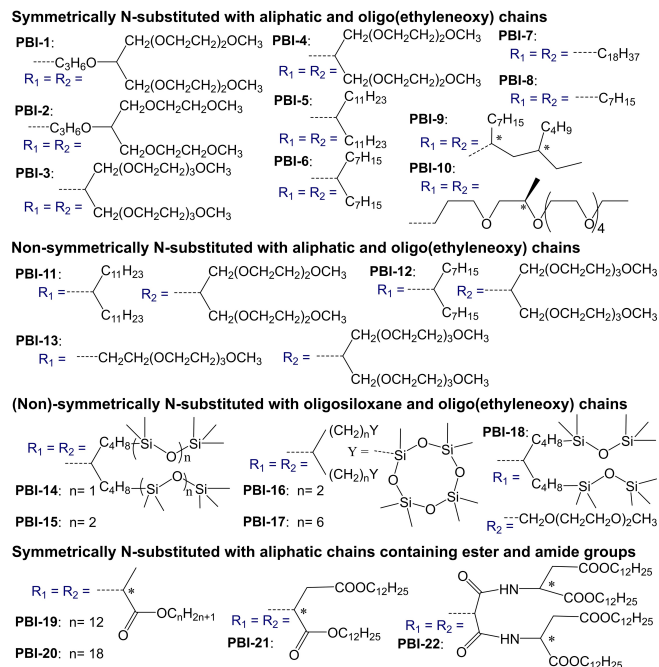


Figure 6. Structures of selected N-substituted PBIs with linear and branched aliphatic, oligo(ethyleneoxy), and oligosiloxane chains as R groups and unsubstituted core ($X=Y=H$) (see Figure 4). Symmetric derivatives have identical R groups attached to the N-positions ($R_1 = R_2$) and nonsymmetric derivatives have two different R groups ($R_1 \neq R_2$). Chiral centres are labelled with an *.

Table 1. Phase transition temperatures and enthalpies for perylene derivatives **PBI-1** to **-22** shown in Figure 6. Cr = crystal, LC = unspecified liquid crystal phase, Col = unspecified columnar mesophase, Col_h = hexagonal columnar mesophase, Col_r = rectangular columnar mesophase, Lam = lamellar mesophase, and I = isotropic liquid.

| Comp. | DSC transition T [°C] and (ΔH [kJ mol ⁻¹]) on heating ^[a] | Ref. |
|---------------|---|---------|
| PBI-1 | Cr -38 (8.4) LC 52–59 (14.2) I | [68,69] |
| PBI-2 | Cr 80 (36.4) LC 167 (17.2) I | [68,69] |
| PBI-3 | Cr 67.8 (24) Col _h 126.9 (3.9) I | [73] |
| PBI-4 | Cr 78.2 (15.8) Col _h 145.8 (3.5) I | [73] |
| PBI-5 | Cr1 53.8 (6.9) Cr2 76.8 (6.6) I | [73] |
| PBI-6 | Cr 133.2 (19.5) I (monotropic Col _h at 118 to 110 °C) | [73] |
| PBI-7 | Cr 180 (15.5) LC 312 (30.7) I | [75] |
| PBI-8 | Cr 214 (24.3) LC ₁ 387 (21.8) LC ₂ 403 (8.8) I ^[b] | [75] |
| PBI-9 | Col 164 (6.3 [J g ⁻¹]) I | [76] |
| PBI-10 | Col 185 (8.27) I | [79] |
| PBI-11 | Cr 51 (10.7) Col _h 107.7 (3) I | [73] |
| PBI-12 | Cr 65.5 (15) Col _h 148.7 (5.9) I | [73] |
| PBI-13 | LC 164 (17.2) I | [67] |
| PBI-14 | LC 47 (1.9 [J g ⁻¹]) LC 138.3 (6.2 [J g ⁻¹]) I | [80,81] |
| PBI-15 | Col _r 122.5 (4.5 [J g ⁻¹]) I | [80,81] |
| PBI-17 | LC 80.1 (4.1 [J g ⁻¹]) I | [82] |
| PBI-18 | Lam 170 (5.8 [J g ⁻¹]) I | [83] |
| PBI-19 | Cr ^[c] 14.6 (19) Lam 198.7 (21.2) I | [84] |
| PBI-20 | Cr 54 Lam 172 I | [9] |
| PBI-21 | Col _h 150 I | [85] |
| PBI-22 | Cr -27 Col _h 181 I | [85] |

[a] Reported phase transitions and assignments are based on DSC (2nd-heating), defect textures obtained by POM, and XRD. [b] Determined from first heating run as the clearing temperature above 400 °C likely coincides with the onset of decomposition. [c] The compound crystallizes from solution and solidifies from the liquid crystal phase as a kinetically trapped partially crystalline material.

attributed to the higher conformational flexibility of the former that lowers melting points more effectively and increases nanosegregation.^[12,72] This was experimentally confirmed by Thelakkat and co-workers who provided a direct comparison between swallow-tailed oligo(ethyleneoxy) chains (**PBI-3** and **PBI-4**) and swallow-tailed alkyl chains (**PBI-5** and **PBI-6**) of similar length (Figure 6 and Table 1).^[73] **PBI-5** is not mesomorph and **PBI-6** displays a monotropic columnar mesophase, whereas **PBI-3** and **PBI-4** show hexagonal columnar mesomorphism over a wide temperature range, as verified by their characteristic fan-shaped and dendritic defect textures with pseudo-isotropic areas (Figure 7a–b). Hansen, Andrienko and co-workers later contributed a detailed study on the differences in molecular dynamics between alkyl and oligo(ethyleneoxy) chains based on solid state NMR measurements and computational studies on **PBI-3** and **PBI-6**.^[74] Shortening of side-chains, either oligo(ethyleneoxy) or alkyl side-chains, expectedly increased phase transition temperatures.^[69,73,75]

While N-substitutions with linear (**PBI-7**, **-8**)^[75] and swallow tail alkyl side-chains (**PBI-5**, **-6**)^[73] of different lengths at best induce monotropic mesomorphism, the use of racemic hyperbranched alkyl chains in **PBI-9** sufficiently lowers melting points to support columnar mesomorphism as demonstrated by Bock and co-workers (Figure 6, Table 1).^[76] Strictly speaking, **PBI-9** is not a single compound but a mixture of ten stereoisomers. This makes it almost impossible for the side-chains to crystallize and extends the mesophase to temperatures well below room temperature. On the other hand, the stability of the mesophase

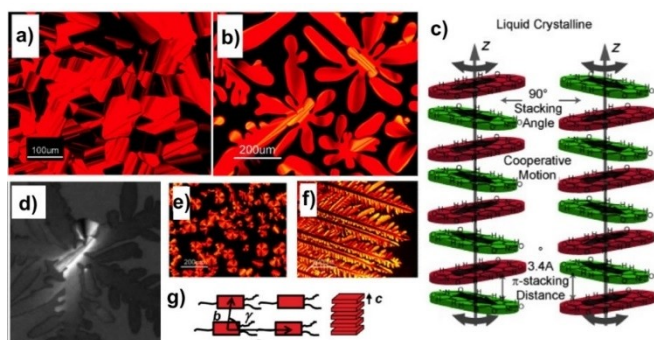


Figure 7. POM images of a) a fan-shaped texture of the Col_h mesophase of **PBI-3** at 142 °C and b) a dendritic growth texture of the Col_h mesophase of **PBI-4** at 144 °C.^[73] c) Schematic of the packing structure and dynamic of the Col_h mesophase of **PBI-3**.^[44] d) POM image of the homeotropically aligned Col_h mesophase of **PBI-9**.^[76] e–f) POM images of Col_h mesophases of **PBI-11** at 108 °C and **PBI-12** at 149 °C showing spherulitic texture with Maltese crosses and dendritic growth.^[73] g) Illustration of the monoclinic unit cell and the resulting columnar packing of non-symmetrically N-substituted **PBI-13**.^[67] Images (a), (b), (e), (f), and (g) are reproduced from Refs. [73] and [67] with permission. Copyright (2013 and 2009, respectively) American Chemical Society. Images (c) and (d) are reproduced from Refs. [44] and [76] with permission. Copyright (2009 and 2016, respectively) Wiley-VCH.

does not depend on order in the side-chain region and its clearing temperature (transition into the isotropic liquid) is much less affected by the mixture of enantiomers and diastereomers. **PBI-9** also has a high propensity for homeotropic alignment as shown in Figure 7d, which is reasoned with an increased fluidity and an advantage for device applications.

Overall, it is astonishing that board-shape molecules with calamitic-like L:B aspect ratios of >5 (Figure 5) form columnar rather than smectic mesophases. To better understand the reasons for this behaviour, **PBI-3** was further investigated by Müllen and co-workers to elucidate the packing structure of its hexagonal columnar mesophase.^[42] A combination of X-ray scattering and solid-state NMR measurements revealed a cooperative rotation about the stacking axis of the PBI molecules in 90° steps (Figure 7c). This orthogonal stacking of the board-shaped molecules reduces steric repulsion between side-chains, allows for a close π - π stacking distance of only 3.4 Å between PBI cores, and better positions the side-chains for the generation of a side-chain continuum around the stacking cores.

Rotation about the stacking axis was highly cooperative to avoid large deviations from the orthogonal correlation between adjacent perylene units in a dynamic mesophase. Accordingly, the lattice parameter of 2.23 nm (distance between columnar stacks) is close to the estimated average of length and breadth for **PBI-3** ($(L+B)/2=2.11$ nm, Figure 5).

All PBIs listed in Figure 6 and most PBIs in general can be expected to pack in similar ways, although the average rotation angle between adjacent PBI units and molecular dynamics will differ depending on the types of side-chains and substitution patterns.^[42] One driving force they all have in common is the relatively strong π - π stacking interaction between electron deficient PBI cores. This and the rotational offset between stacking PBI cores has been reasoned with

dipolar interactions between imide groups^[75] and multipolar interactions between PBI cores (see electrostatic surface potential maps in Figure 5).^[77] However, polytopic interactions^[78] may also contribute and the out-of-plane orientation for many substituents at bay- and N-positions require rotational offset for small stacking distances.

Meijer and co-workers achieved room temperature columnar mesomorphism with just one long chiral oligo (ethyleneoxy) chain at each N-position in **PBI-10**.^[79] In this case, the columnar arrangement is supported by the induction of supramolecular chirality rather than the suppression of crystallization by the formation of mixtures of enantiomers and diastereomers for compounds with racemic chiral centres such as **PBI-9**.

Finally, mesomorphism may be controlled by the attachment of different side-chains to each N-position, which generates PBIs of lower symmetry.^[67,73] While PBIs bearing two different types of alkyl substituents are crystalline and do not display liquid crystal phases, PBIs with swallow-tail substituents that contain one oligo(ethyleneoxy) and one alkyl chain (e.g. **PBI-11** and **PBI-12**) display thermotropic columnar mesophases over a wide temperature range. Their defect textures were indicative of Col_h mesophases (Figure 7e–f) although a nanosegregation between the two immiscible types of side-chains should be expected that favours lamellar over columnar lattices and disfavours a hexagonal columnar lattice.^[73] Apparently, the larger packing volumes of the side-chains at both sides sufficiently disfavour lamellar packing. In contrast, a lamellar columnar packing structure is observed for PBIs substituted with one linear and one swallow-tail oligo (ethyleneoxy) chain.^[67] An example is **PBI-13**, which crystallizes in an oblique unit cell (Figure 7g) and its lamellar phase aligns on substrates preferentially with an edge-on orientation of the molecules as revealed by XRD. The formation of a lamellar (no interfacial curvature) rather than a columnar supramolecular structure is reasoned with an alternating alignment of the molecules that generates a balanced packing volume for both sides of the side-chain layers.

Oligo(ethyleneoxy) chains are not only excellent building blocks for the design of mesomorphic PBIs, but also have a high dielectric constant for organic materials,^[86] good solubility in polar solvents, and support ion conductivity.^[87] However, some of these properties also cause challenges such as their ability to chelate various cations and incorporate other impurities.

For this and other reasons different types of side-chains have been studied for the generation of mesomorphic PBIs. Funahashi and co-workers studied unbranched and swallow-tailed alkyl chains with linear and cyclic oligosiloxane end groups as new types of side-chains for N-substituted PBIs.^[80–82] Oligosiloxane chains are similarly flexible and microphase segregate equally well as oligo(ethyleneoxy) chains but, in contrast to oligo(ethyleneoxy), do not easily trap ionic impurities and improve solubility only in nonpolar solvents. Derivatives with swallow-tailed side-chains and terminal disiloxane (**PBI-14**) and trisiloxane (**PBI-15**) chains both exhibited columnar liquid-crystallinity whereas PBI derivatives with just one linear alkyl-siloxane chain at each end formed higher ordered lamellar

mesophases.^[80,81] However, the larger packing volume of siloxane chains compared to alkyl and oligo(ethyleneoxy) chains interfere with the π - π stacking of the PBI cores based on XRD, although the low temperature rectangular columnar mesophase of **PBI-14** reached a high charge carrier mobility of $0.1 \text{ cm}^2 \text{ V}^{-1} \text{ s}^{-1}$ measured by a time-of-flight method, which indicates good electronic interactions between the PBI cores.

The same group investigated swallow-tailed alkyl chains with terminal cyclotetrasiloxane groups as an unusual attempt to increase the lateral packing volume of the chains and introduce polymerizable side-chains.^[82,88] The derivative **PBI-16** with short dimethylene spacers was not liquid-crystalline but hexamethylene spacers induced a disordered rectangular columnar mesophase for **PBI-17**. The latter still showed a respectable electron mobility of $10^{-2} \text{ cm}^2 \text{ V}^{-1} \text{ s}^{-1}$ that is in-between the maximum values obtained for **PBI-14** and **PBI-15**.

Finally, Funahashi and co-workers experimented with the non-symmetric attachment of a swallow tail alkyl-siloxane chain at one N-position and a linear oligo(ethyleneoxy) chain at the other.^[83] This suppressed crystallization and, consequently, widened the temperature range of the mesophase of **PBI-18** well below room temperature. The authors proposed the formation of a lamellar rather than a columnar mesophase based on diffraction data, which was reasoned with a nano-segregation between the two types of side-chains and their largely differing packing volumes that cannot be easily accommodated in a columnar mesophase.

Another option for tuning the mesomorphism of N-substituted PBIs is the incorporation of functional groups other than ethers. This was accomplished for **PBI-19** to **PBI-22** by the incorporation of ester groups and a combination of ester and amide groups for **PBI-22** (Figure 6 and Table 1).^[9,84,85] Ester groups are expected to lower transition temperatures because of their steric flexibility but they also introduce directional dipole-dipole interactions that can increase transition temperatures and affect molecular shape. In addition, all four derivatives are pure enantiomers as the chiral linking groups at the N-positions are L-alanine for **PBI-19** and **-20** and L-aspartic acid for **PBI-21** and **-22**.

Compounds **PBI-19** and **-20** with only single, linear alkyl chains on each side demonstrate how powerful the ester groups are in promoting mesomorphism, although both compounds appear to form lamellar rather than columnar mesophases. This is not surprising as filling the side-chain continuum of columnar stacks with just two linear aliphatic chains per molecule is unfavourable. Despite their lamellar structures, both PBIs show a strong X-ray diffraction peak for π - π stacking at 3.4 \AA , which is why **PBI-20** was tested as an organic semiconductor in photovoltaic devices.^[9] Detailed X-ray diffraction studies on thin films of **PBI-19** suggest the edge-on molecules stack with alternating tilt with regard to the normal of the substrate.^[84]

PBI-21 and **-22** have two and four dodecyl esters on each side, respectively, which is sufficient for biasing their self-organization towards columnar mesomorphism.^[85] **PBI-21** does not crystallize and the clearing temperature of its Col_h mesophase is lowered to 150°C . The Col_h mesophase of **PBI-22**

is 30°C more stable than that of **PBI-21** and does crystallize, albeit at -27°C . Clearly, intermolecular H-bonds between the four amide groups more than compensate for twice the number of ester groups and dodecyl chains and their directionality seems to aid crystallization. Similarly low melting points have been observed in other columnar mesophases with strong intracolumnar H-bonding but crystallization may also be hindered by H-bonding.^[89]

Most of the PBIs discussed so far have overall rod-shaped structures that generate either lamellar or columnar mesophases (Figure 5). Exceptions are **PBI-17** and **-22** because the lateral packing volume of their side-chains is much larger than that of the core. Consequently, the breadth of the compound is now dictated by the lateral packing of the side-chains rather than the core (Figure 8). Their structures are better described as dumbbell-shaped instead of rod-shaped and strongly bias columnar over lamellar arrangements. Their aspect ratio $L:B$ varies depending on what value is used for B as the value of B changes with the location of the measurement.

In **PBI-17** and **-22** the lateral packing volume was increased by either using cyclic structures or the attachment of 4 side-chains on each side (octacatenane structure), respectively. Wedge- to cone-shaped 3,4,5-trialkoxypheyl and 3,4,5-trialkylphenyl groups are more frequently applied as large mesogenic side-chain groups in liquid crystal research and they have also been widely applied for the derivatization of PBIs at their N-positions. Examples **PBI-23** to **-45** contain one at each N-position to give derivatives with 6 side-chains often called hexacatenanes (Figure 9 and Table 2). Both, the packing volume of three side-chains at each N-position and the wedge- or cone-shape of these groups highly favour columnar (higher interfacial curvature) over lamellar mesomorphism, although the in-plane aspect ratio does not significantly decrease unless the breadth

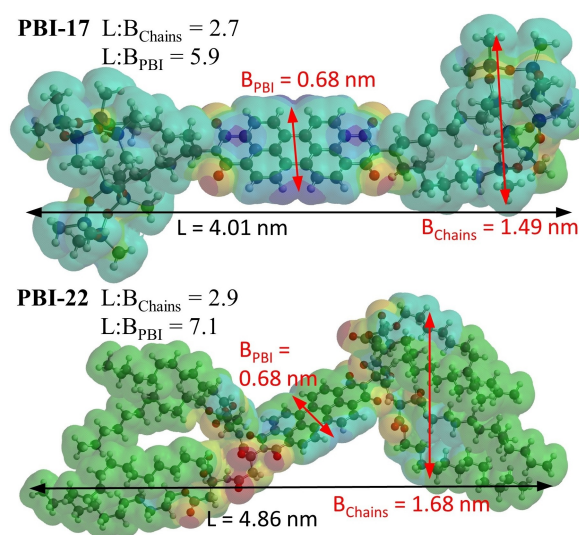


Figure 8. Electrostatic potential maps projected onto density surfaces generated by semiempirical PM6 calculations (Spartan) for dumbbell-shaped **PBI-17** and **PBI-22** in the gas phase. In-plane aspect ratios are provided based on estimated overall lengths of the molecule for side-chains in amorphous states and two different breadth values for the PBI core and side-by-side packed side-chains.

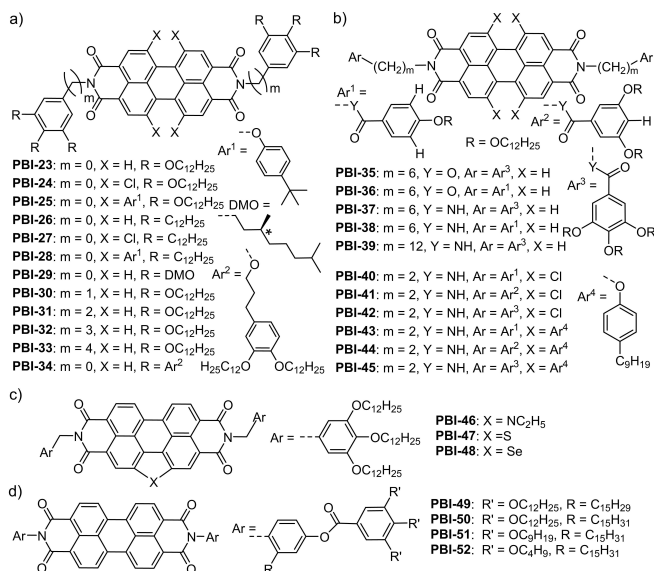


Figure 9. Structures of selected PBIs with a) trialkoxyphenyl or trialkylphenyl substituents at the N-positions, b) alkoxy benzoic ester and benzamide groups, c) mono bay annulation and d) trialkoxy benzoic ester with 3-pentadecyl phenol (cardanol derivative) spacers. Some PBIs have alkyl spacers of variable length between the N-position of the PBI and the terminal aromatic group and some are bay-substituted or -annulated.

is measured at the wide end of the wedge. In some instances, the bay positions were also substituted, which not only decreases the in-plane aspect ratio but also distorts the perylene core from planarity to improve solubility and lower phase transition temperatures.

A large body of related work has been contributed by Würthner and co-workers. **PBI-23** to **PBI-28** possessed 3,4,5-trialkoxypheyl and 3,4,5-trialkylphenyl N-substituents with long alkyl chains (often dodecyl).^[7,46,77,90–92] **PBI-23** forms a disordered Col_h mesophase (Figure 10a) from room temperature up to a very high clearing point of 373 °C.^[77] The same compound but bay-chlorinated (**PBI-24**) displays an ordered Col_h mesophase with a reduced temperature range from 86–214 °C. The reduced temperature range is expected since the bay-substitution twists the PBI core, which typically reduces π - π interactions (Figure 10b–c).^[90] Unexpectedly, the improved stacking order of the chlorinated derivative, as suggested by XRD, does not manifest itself in a higher charge carrier mobility for **PBI-24** when compared to the less ordered **PBI-23**. However, bay-chlorination increases the charge carrier lifetime by more than 100 times.

Notably, no fluorescence is observed for solutions and aggregates of **PBI-23** and **PBI-24**, and this is reasoned with photoinduced electron transfer from the electron-rich trialkoxyphenyl groups to the electron-deficient perylene core.^[46,77] On the other hand, **PBI-25** and **PBI-28** with electron-rich phenoxy groups at their bay positions show fluorescence enhancement in solution.^[7,77] In contrast, fluorescence in condensed phases is not just a molecular property but strongly affected by supramolecular structures that dictate intermolecular interactions. Polymorphic **PBI-27**, for example, displays a non-

Table 2. Phase transition temperatures and enthalpies for perylene derivatives shown in Figure 9. Cr = crystal, Col = unspecified columnar mesophase, $Col_{h,d}$ and $Col_{h,o}$ = hexagonal columnar mesophases with disordered and ordered intracolumnar stacking, respectively, $Col_{h,p}$ = higher ordered plastic hexagonal columnar mesophase, Lam = lamellar mesophase, LC = unspecified liquid crystal phase, I = isotropic liquid, and BCC = body-centred cubic phase.

| Comp. | DSC transition T [°C] and (ΔH [kJ mol ⁻¹]) on heating ^[a] | Ref. |
|---------------|---|-------|
| PBI-23 | $Col_{h,d}$ 373 (8.9) I | [77] |
| PBI-24 | Cr 86 (61 [J g ⁻¹]) Col_h 214 (14 [J g ⁻¹]) I | [90] |
| PBI-25 | Col_h 346 (15) I | [77] |
| PBI-26 | Col_h 300 (12.5 [J g ⁻¹]) I | [92] |
| PBI-27 | $Col_{f,o}$ 110 (8.4) I ^[b] | [7] |
| PBI-28 | Col_h 285 (23.5) I | [7] |
| PBI-29 | Col_h 349 (28.0) I | [92] |
| PBI-30 | Col_h 225 (16.9) I | [94] |
| PBI-31 | Cr -20 (18.3) Col_h 134 (1.3) I | [94] |
| PBI-32 | Cr 84 (1.9) Col_h 125 (2.5) I | [94] |
| PBI-33 | Cr 87 (0.6) Col_h 113 (2.8) I | [94] |
| PBI-34 | Cr 18 Col_h 124 Col_h 157 BCC 211 I | [95] |
| PBI-35 | LC ^[c] 137 (39.1 [J g ⁻¹]) I | [96] |
| PBI-36 | Cr 73.8 (0.5 [J g ⁻¹]) Lam 229.0 (35.5 [J g ⁻¹]) I | [96] |
| PBI-37 | Cr 36.9 (3.9 [J g ⁻¹]) LC ^[c] 131.5 (16.8 [J g ⁻¹]) I | [96] |
| PBI-38 | Cr 146.2 (21 [J g ⁻¹]) Col 249.0 (16.1 [J g ⁻¹]) I | [96] |
| PBI-39 | Cr 91.5 (0.9 [J g ⁻¹]) LC ^[c] 172.7 (22.5 [J g ⁻¹]) I | [96] |
| PBI-40 | Cr 87.2 (13.1) Col_h 228.4 (10.4) I | [97] |
| PBI-41 | Cr 85.6(10.6) Col_h 216.3(9.8) I | [97] |
| PBI-42 | Cr 80.0 (14.3) Col_h 208.1 (12.2) I | [97] |
| PBI-43 | Cr 68.8 (13.3) Col_h 198.1 (6.9) I | [97] |
| PBI-44 | Cr 56.5 (14.4) Col_h 177.8 (5.2) I | [97] |
| PBI-45 | Cr 40.2 (16.8) Col_h 151.6 (4.5) I | [97] |
| PBI-46 | $Col_{h,1}$ 77.8 (0.7) $Col_{h,2}$ 156.1 (1.4) I | [98] |
| PBI-47 | Col_h 200.6 (2.3) I | [98] |
| PBI-48 | Cr 78.6 (2.3) Col_{ob} 125.1 (9.4) Col_h 202.5 (2.2) I | [98] |
| PBI-49 | Cr 29 (42.8) Col_h 195 (6.2) I | [99] |
| PBI-50 | Cr 20 (60.5) $Col_{h,p}$ 167 (5.8) Col_h 215 (16.7) I | [99] |
| PBI-51 | Cr 202 (33.22) I ^[d] | [100] |
| PBI-52 | Cr 264 (72.83) I | [100] |

[a] All phase assignments are based on DSC analysis, defect textures obtained by POM, and XRD data. [b] A Cr to Cr transition was observed in the first heating run. [c] Unidentified mesophase of likely columnar structure. [d] A monotropic Col_h phase is obtained on cooling at about 190 °C.

fluorescent *H*-aggregation like packing in its crystalline phase and a strongly fluorescent *J*-aggregation like packing in its columnar mesophase (Figure 10c).^[7]

Exchange of trialkoxyphenyl with trialkylphenyl groups in **PBI-26** to **PBI-32** reduces clearing temperatures (thermal stability) of their columnar mesophases in comparison to their respective counterparts **PBI-23** to **PBI-25**. This agrees with a generally observed destabilization of columnar mesomorphism in compounds with two or more alkyl groups directly attached to aromatic rings in ortho-positions. This has been explained with a decrease in steric flexibility at the linking point that pushes chains into out-of-plane orientations.^[93]

Chirality, on the other hand, usually stabilizes columnar mesomorphism. This can be seen in **PBI-29**, which displays a high clearing temperature of 349 °C for its ordered Col_h mesophase despite its branched side-chains. Its high stacking order is also manifested in an increased charge carrier mobility when compared to the disordered Col_h phases of **PBI-23** and **PBI-26**.^[92]

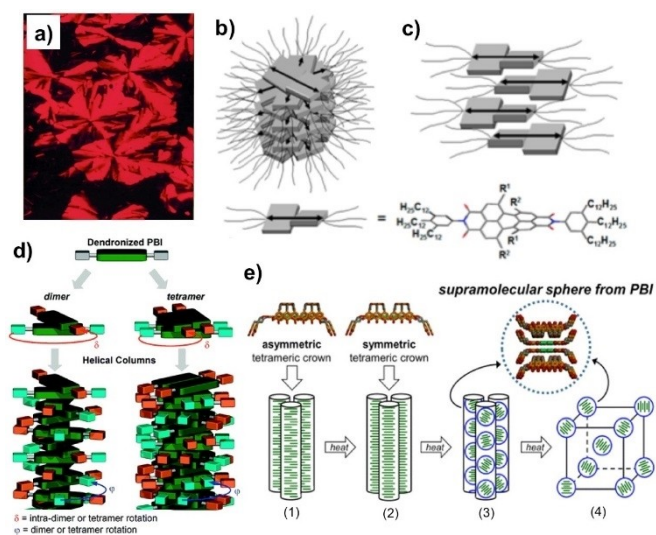


Figure 10. a) POM image of fan-shaped texture of Col_h mesophases of **PBI-23**.^[77] b–c) Schematic representation of packing structures proposed for the columnar mesophase of **PBI-27** with *H*-aggregation like packing (b) and its crystalline structure with *J*-aggregation like packing (c).^[7] d) Schematics of the helical columnar mesophases of **PBI-30** ($m = 1$), consisting of stacked dimers, and of **PBI-23** and **PBI-31** to **PBI-33** ($m = 0, 2, 3, 4$) consisting of stacked tetramers.^[94] e) Schematic representation of the four mesophases displayed by **PBI-34** upon heating; (1) crystalline columnar hexagonal phase, (2) low temperature Col_h mesophase with intracolumnar order, (3) high temperature Col_h phase containing small spherical aggregates, (4) body-centred cubic mesophase of small spherical aggregates.^[95] Images (a–c) are reproduced from Refs. [77] and [7] with permission. Copyright (2001 and 2007, respectively) Wiley-VCH. Images (d) and (e) are reproduced from Refs. [94] and [95]. Copyright (2011 and 2016, respectively) American Chemical Society.

A collaborative effort by the groups of Percec, Spiess, Ungar, and Heiney, and other co-workers led to a remarkably detailed structural characterization of the complex mesomorphism displayed by perylene bisimides N-substituted with oligomethylene spacers of 1 to 4 carbon atoms that are terminated with 3,4,5-trialkoxybenzene groups.^[94,101,102] Standard characterization of their mesophase structures by polarized optical microscopy (POM), thermal analysis (DSC), and variable temperature X-ray diffraction was enhanced by X-ray diffraction on aligned fibre samples, molecular modelling, comparisons with predicted diffraction patterns, and solid-state 1H NMR measurements that provided information on the molecular dynamics within the NMR time scale. All compounds were found to self-organize into columnar stacks with specific rotational angles between stacking molecules as discussed earlier for other N-substituted PBI derivatives.

Variation of the oligomethylene spacer significantly affects the intracolumnar packing structures for derivatives with 3,4,5-tridodecyloxybenzene groups (**PBI-23** and **PBI-30** to **PBI-33** for $m = 0–4$), although all compounds display ordered hexagonal columnar mesophases as high temperature mesophases.^[94] Their crystalline columnar structures at lower temperature have orthorhombic unit cells, except for the monoclinic phase of **PBI-30** ($m = 1$). **PBI-30** also differs in its columnar packing structures with only one molecule in each repeat unit of the monoclinic columnar phase (Figure 10d) and all molecules of one column

facing up or down. This changes in the hexagonal columnar mesophase that contains pairs of up and down facing molecules. This drastic change in packing structure explains why the transition from the Col_h mesophase to the columnar crystal phase is kinetically extremely slow.

In contrast, PBIs with $m = 0, 2, 3$, and 4 arrange into side-by-side pairs of two molecules that stack into tetramers as basic repeat units (Figure 10d). One pair is turned upside-down and rotated around the column axis with regard to the other pair. The rotation angles differ for different values of m .

Clearing temperatures of **PBI-23** and **PBI-30** to **PBI-33** decrease with increasing spacer length (m) but their melting temperatures increase. The latter is probably caused by differences in crystallization kinetics. Longer spacer units provide faster crystallization kinetics because they generate more flexibility and fluidity while the crystallization kinetics for **PBI-23** is extremely slow and was not observable by DSC at the chosen conditions. A more detailed study of crystallization kinetics and self-healing processes was provided for compounds **PBI-30** and **PBI-32** with alkyl chains of different lengths.^[101,102]

Finally, attachment of sterically more demanding conical dendritic groups with six dodecyloxy chains directly to the N-positions ($m = 0$) in **PBI-34** (Figure 9a) caused the self-organization into unprecedented close to spherical crown-shaped tetramers.^[95] At low temperature, these tetramers self-organize into columnar mesophases that break up into columnar stacks of spherical units at elevated temperature that eventually rearrange into a body-centred cubic (BCC) mesophase as illustrated in Figure 10e.

The spacer length between trialkoxyphenyl groups and the N-positions of the PBI critically affect the self-organization of **PBI-23** to **PBI-34** also because it alters the relative orientation of the trialkoxyphenyl groups with regard to the PBI core and its conformational dynamics. The associated increase in aspect ratio with the small increases in spacer length has likely comparatively little effect on the phase transition temperatures.

Much longer spacers of 6 and 12 methylene groups were used by Asha and co-workers in compounds **PBI-35** to **PBI-39** with dodecyloxy and tridodecyloxy benzoate and benzamide terminal groups (Figure 9b).^[96] Their work mainly focused on the aggregation and fluorescence of these compounds, but they did include a preliminary report on their mesomorphism (Table 2). They proposed a lamellar mesophase (*J*-type aggregates) for **PBI-36** and a columnar mesophase (*H*-type aggregates) for **PBI-38**. The latter is induced by H-bonding between amide groups and despite the presence of only two dodecyloxy chains. They also reported mesomorphism for the parent PBI derivatives without alkoxy chains that are not shown here.

Recently, Guo, Yang, and co-workers expanded the body of work on benzamide N-terminated PBI derivatives by reporting non-planar bay-substituted **PBI-40** to **PBI-45** with short dimethylene spacers (Figure 9b).^[97] Surprisingly, compounds **PBI-40** and **PBI-43** with only two dodecyloxy side-chains form columnar mesophases, although the broadness of the (d_{10}) X-ray reflection indicates a rather short range packing order for the columnar lattice (Table 2). The highest intercolumnar packing order is observed for **PBI-44** and **PBI-45** that have 4-non-

ylphenoxy groups at their four bay positions and generate much lower in-plane aspect ratios and discotic-like overall shapes (Figure 11). Thermal transition temperatures expectedly decrease with increasing number of side-chains, but the differences in transition temperatures are surprisingly small considering the large differences in number of alkyl chains. Perhaps, it is the H-bonding between amide groups that dominates the values of transition temperatures.

The effect of bay-annulation of **PBI-30** with heteroatoms on its self-assembly was studied by Gupta and co-workers (**PBI-46** to **PBI-48**, Figure 9c and Table 2).^[98] A red-shifted absorption of the N-ethyl annulated derivative **PBI-46** in comparison to **PBI-30** is reasoned with an enhanced *J*-type character of the aggregates, whereas the S-annulated **PBI-47** and Se-annulated **PBI-48** exhibit a small blue-shift, indicating a change to more *H*-type aggregates.

All three PBIs exhibit Col_h mesomorphism like **PBI-30**, but the Se-annulated derivative **PBI-48** displays an additional low-temperature oblique columnar mesophase (Col_{ob}). The observation of a Col_{ob} phase is reasoned with enhanced intermolecular interactions between **PBI-48** molecules due to the large and more polarizable Se atom. Overall, mono bay-annulation lowers melting and clearing temperatures and increases solubility in comparison to the parent **PBI-30**, most likely because of the lowered symmetry.

Core elongation in **PBI-49** and **PBI-50** is achieved by linking terminal tridodecyloxybenzoyl groups *via* rigid cardanol and 3-pentadecyl phenol spacer groups, respectively, to the N-positions of PBI (Figure 9d).^[99] This elongation would likely result in lamellar mesomorphism in the absence of the lateral side-chains on the phenol linker. The presence of these lateral

chains sufficiently disturbs smectic packing and reduces the in-plane aspect ratio to support columnar mesomorphism (Table 2). **PBI-50** displays strong π - π stacking interactions in its Col_h mesophase that are apparently absent in the Col_h mesophase of **PBI-49** containing a sterically more demanding C=C double bond with Z-configuration in its side-chain.

A stepwise reduction of the length of the alkoxy chains from dodecyl to butyl (two examples are **PBI-51** and **PBI-52** in Figure 9d) reveals nonyl as the minimum chain length required for monotropic columnar mesomorphism to occur, and dodecyl chains as the minimum length for enantiotropic mesomorphism to occur.^[99,100] The monotropic columnar mesophases of derivatives with side-chains of 9 to 11 carbon atoms likely have rectangular structures (Col_r) based on preliminary XRD data. The dodecyl substituted **PBI-50** gives the highest charge carrier mobility of $10^{-3} \text{ cm}^2 \text{ V}^{-1} \text{ s}^{-1}$ for all derivatives measured by the space-charge-limited current method.

All previously discussed PBIs have their N-positions substituted with side-chains and other groups to avoid strong H-bonding interactions between their imide groups. Lehmann's and Würthner's groups decided to take advantage of the strong and directional H-bonding interactions and investigated the thermotropic behaviour and supramolecular self-assembly of tetra-bay substituted PBIs **PBI-53** to **PBI-56** in Figure 12a and Table 3.^[103,104] Their H-bonding dictates an end-to-end interaction between imide groups that orients the long axis of the PBIs about parallel to the column axis (Figure 12b), rather than perpendicular or otherwise tilted as in all previous examples of mesomorphic PBIs. The twisted core structures induce helical self-organization in the columnar mesophases of **PBI-54** to **PBI-**

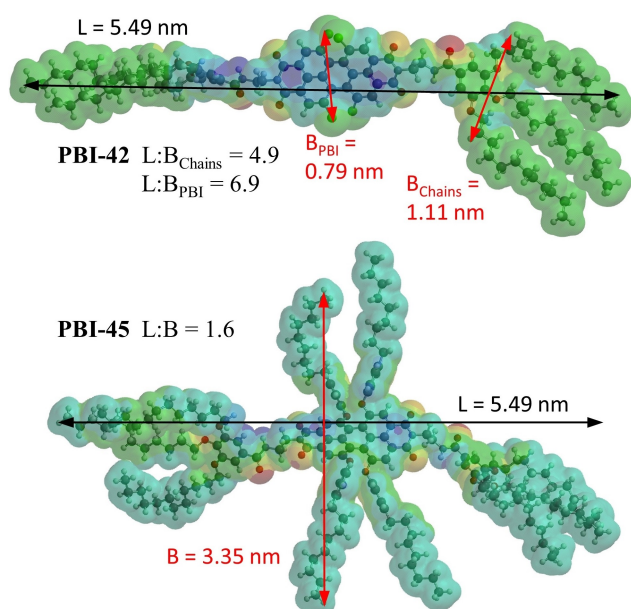


Figure 11. Electrostatic potential maps projected onto density surfaces generated by semiempirical PM6 calculations (Spartan) for non-planar **PBI-42** and **PBI-45** in the gas phase. In-plane aspect ratios are provided based on estimated overall lengths and breadths of the molecules for side-chains in amorphous states. Two different breadth values are given for **PBI-42** as the PBI core and the side-by-side packed side-chains generate different values.

Table 3. Phase transition temperatures and enthalpies for perylene derivatives shown in Figures 12–15. Cr = crystal, Col_h = hexagonal columnar mesophase, Col_r = rectangular columnar mesophase, Col_p = plastic crystalline columnar mesophase, Col_{glass} = columnar mesophase frozen in as an anisotropic glass, and I = isotropic liquid.

| Comp. | DSC transition T [°C] and (ΔH [kJ mol ⁻¹]) on heating ^[a] | Ref. |
|---------------|---|-------|
| PBI-53 | Cr 150 (13.29) I | [103] |
| PBI-54 | Col_r 210 (5.5) Col_h 252 (7.83) I | [103] |
| PBI-55 | Col_h 235 (7.78) I | [103] |
| PBI-56 | Cr -25 (2.38) Col_h 279 (9.88) I | [103] |
| PBI-57 | Cr 278 (31.4) I | [106] |
| PBI-58 | Col_p 188 (7.52) Col_h > 500 I | [106] |
| PBI-59 | Col_p 285 (17.6) I | [106] |
| PBI-60 | Cr 236 (24.4) I ^[b] | [107] |
| PBI-61 | Cr 282 (68.7) I ^[c] | [107] |
| PBI-62 | Cr 202 (18.7) I ^[c] | [107] |
| PBI-63 | Cr 61.8 (10.6) Col_h 162.9 (13.8) I | [108] |
| PBI-64 | Cr 53.3 (12.2) Col_h 190.5 (11.1) I | [108] |
| PBI-65 | Cr 43.6 (12.4) Col_h 222.1 (19.3) I | [108] |
| PBI-66 | Cr 32.4 (16.6) Col_h 234.3 (23.8) I | [108] |
| PBI-67 | Cr 41.3 (16.9) Col_h 202.8 (18.8) I | [109] |
| PBI-68 | Cr 72.8 (12.5) Col_h 219.1 (13.7) I | [109] |
| PBI-69 | Cr 86.8 (11.7) Col_h 214.6 (7.9) I | [109] |
| PBI-70 | Cr 107.1 (10.9) Col_h 231.4 (6.8) I | [109] |
| PBI-71 | Col_{glass} 84 (T_g) Col_h 146 (4.0 [J g ⁻¹]) I | [110] |
| PBI-72 | Col_{glass} 52 (T_g) Col_{ob} 159 (5.9 [J g ⁻¹]) I | [110] |

[a] All phase assignments are based on DSC analysis, defect textures obtained by POM, and XRD. [b] potential metastable smectic and [c] nematic phase.

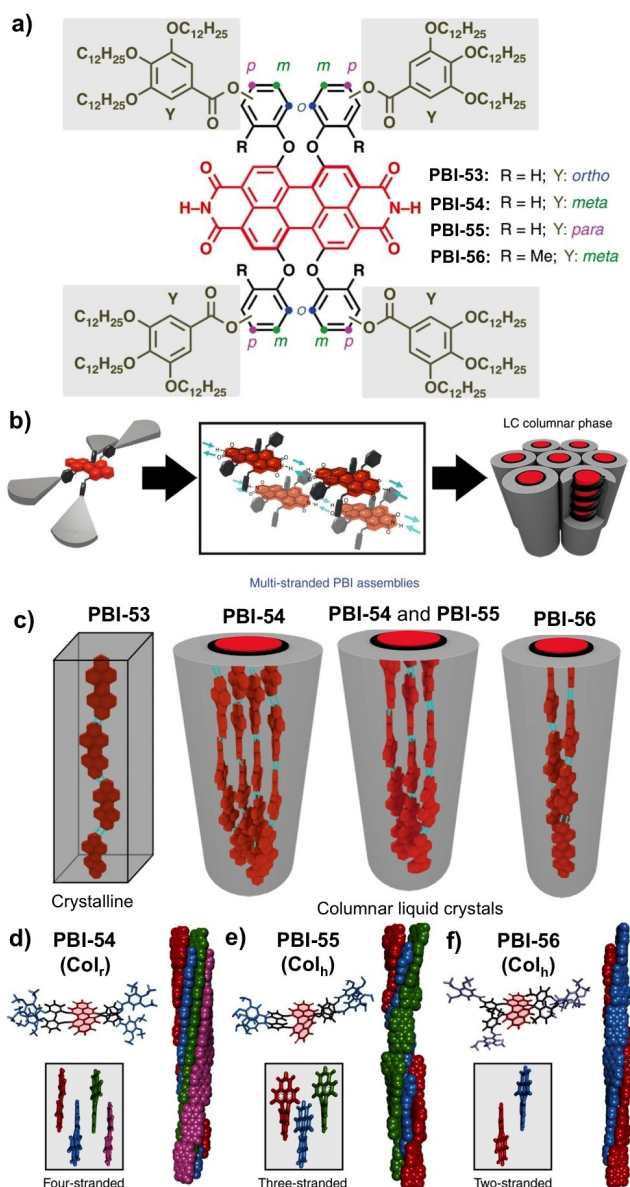


Figure 12. a) Chemical structure of tetra-bay phenoxy-dendronized PBIs (PBI-53 to PBI-56). (b–e) Schematic representations of b) the self-assembly of the PBIs via H-bonding and π - π interactions, c) the assemblies of PBIs into one, two, three, or four strands, with PBI-53 being crystalline and PBI-54 to PBI-56 being liquid crystalline, and (d–e) the optimized self-assembled structures of the liquid crystalline PBIs (PBI-54 to PBI-56) into tetramers, trimers, and dimers, respectively.^[103] Reproduced from Ref. [103] with permission under the terms of the Creative Commons license. Copyright (2018) Nature Publishing Group.

56 and their side-chain continuum is filled by the tridodecyloxy benzoic ester groups laterally attached to the bay positions.

How many strands form one columnar unit (2, 3, or 4) is controlled by the position of the benzoic ester groups at the phenoxy spacer (*ortho*, *meta*, or *para*) and the type of R-group as illustrated in Figures 12c–f.^[103] Within each strand, the PBI cores generate electronically coupled *J*-type aggregates with slipped π - π interactions in their crystalline and liquid crystalline phases. Overall, the number of strands per column is dictated by steric congestion, nanosegregation, and space-filling require-

ments and this design has been used to generate core-shell columnar structures.^[105]

Only a few examples of PBI derivatives with enlarged conjugated cores are covered here to highlight general trends. Müllen and co-workers provided an instructive comparison between core extensions along the long axis (*longitudinal extension*) in terylene and quaterylene diimides PBI-57 and PBI-58, respectively, and along the short axis (*lateral extension*) in coronene diimide PBI-59 (Figure 13a and Table 3).^[106] The enlargement of the aromatic core generates stronger π - π interactions that increase clearing points without affecting thermal stability. The enhanced π - π stacking decreases the molecular dynamics of the mesophase and overall improves charge carrier mobility. Optically, the long-axis extensions bathochromically shift the longest wavelength absorption all the way to 760 nm for PBI-58, whereas the short-axis extension causes a hypsochromic shift to 430 nm for PBI-59 when compared to the parent PBI-6 (Figure 13b).

Differences were also noted in the mesomorphism of the differently sized and shaped cores. Terylene diimide PBI-57 is crystalline and not mesomorph, like PBI-6, and forms highly ordered domains with edge-on orientation on substrates. This is a property particularly interesting for organic field-effect transistors (Figure 13c). Quaterylene diimide PBI-58 also favours edge-one alignment on substrates but displays a low temperature plastic crystalline mesophase (Col_p) and a high temperature Col_h mesophase. In contrast, disc-shaped coronene diimide PBI-59 aligns homeotropically (planar) on substrates and displays a plastic columnar mesophase (Figure 13d).^[106]

It is noted here that a series of liquid-crystalline coronene bisimides was investigated by Marder and co-workers and they reported an exceptionally high SCLC charge carrier mobility of $6.7 \text{ cm}^2 \text{ V}^{-1} \text{ s}^{-1}$ for the *N,N'*-bis(pentadecylfluorooctyl)-substituted derivative.^[111] Recent work on new PBI-like derivatives with extended aromatic cores that formed columnar mesophases has been reported by the Bock group.^[112–114]

PBIs have also been covalently linked together or attached to other mesogenic groups to control their self-assembly, supramolecular chemistry, and mesomorphism. An interesting

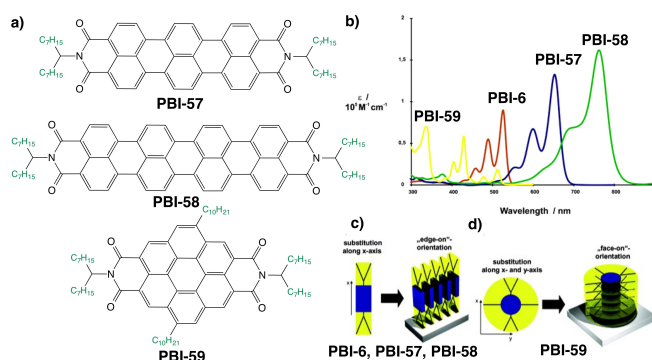


Figure 13. a) Structure of core-extended PBIs (PBI-57 to PBI-59). b) Absorption spectra upon core extensions compared to their counterpart PBI-6. c) Schematic illustration of the arrangement on surfaces for terylene diimides (PBI-6, PBI-57 and PBI-58) with "edge-on" orientation, versus d) for coronene diimide (PBI-59) with "face-on" orientation.^[106] Images (b–d) from are adapted from Ref. [106]. Copyright (2006) American Chemical Society.

approach is the coupling of two PBI molecules between N-positions by methylene spacers. Asha and co-workers studied dimers with methylene spacers of one to twelve carbon atoms and examples are compounds **PBI-60** to **-62** with spacers of one, six, and twelve carbon atoms (Figure 14 and Table 3).^[107]

The authors claimed the formation of a smectic-like mesophase for **PBI-60** and nematic mesophases for most of the other derivatives, although transition enthalpies suggest the presence of higher ordered mesophases. Clearly, the single short ethylhexyl side-chain at each terminal N-position does not support columnar mesomorphism and the two lateral pentadecyl chains should also destabilize lamellar packing but are essential for lowering melting points. Changes in phase behaviour with varying spacer length and the observed distinct odd-even effect agree with what has been reported for other calamitic dimers.^[115,116]

Covalent attachment of calamitic mesogens to PBI chromophores has been explored by the groups of Guo and Yang.^[108,109] Both studied PBIs that contain cholesterol units at bay- and N-positions (**PBI-63** to **-70** in Figure 14 and Table 3).

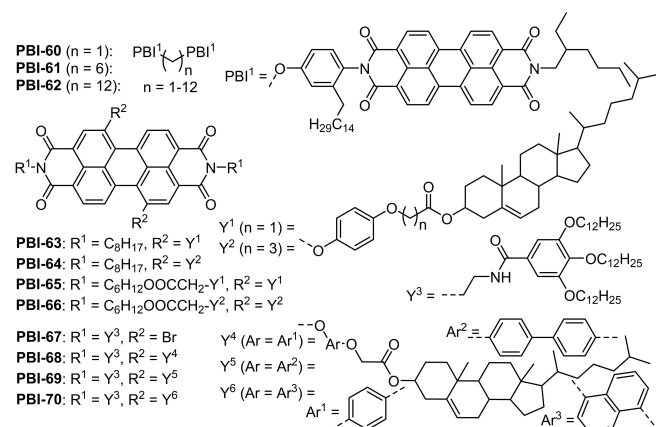


Figure 14. Molecular structures of **PBI-60** to **PBI-70**.

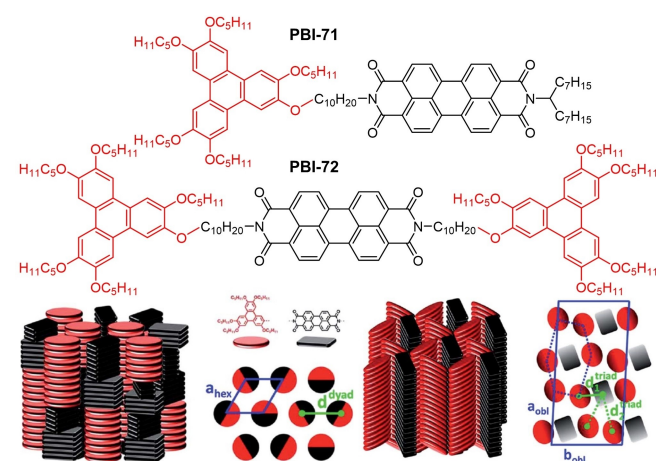


Figure 15. a) N-substitution of PBI with one or two discotic triphenylene units generates donor-acceptor dyad **PBI-71** and triad **PBI-72**, respectively. b) Proposed packing structure of **PBI-71** in its Col_h mesophase. c) Proposed packing structure of **PBI-72** in its Col_{obl} mesophases.^[117] Reproduced from Ref. [117] with permission. Copyright (2016) Royal Society of Chemistry.

Overall, attachment of the calamitic cholesterol groups to the bay positions of the PBIs significantly lowers the in-plane aspect ratios and melting points and both effects enhance columnar mesomorphism. Only one bay-position on each side is substituted, which significantly lowers the distortion of the PBI core and steric interference with π - π stacking interactions. All compounds are highly fluorescent in solution with fluorescence quantum yields of >0.9 but barely fluorescent in their condensed phases, which is an indication for *H*-type aggregation in the columnar stacks.

Finally, PBIs can be linked to discotic liquid crystals. Several groups have worked on dyads and triads of PBIs N-substituted with one or two alkoxytriphenylenes for the construction of segregated columns of acceptor PBI and donor triphenylene units (Figure 15).^[110,117–119] Two examples are dyad **PBI-71** and triad **PBI-72** of which the triad indeed self-organizes into separate columns of PBI acceptor and triphenylene donor molecules in an oblique columnar lattice. The dyad arranges into a hexagonal columnar mesophase with each column containing stacks of both donor and acceptor molecules. Surprisingly, the donor and acceptor moieties are not stacked alternately or distributed randomly in each columnar stack. Instead, the authors propose a segregation into alternating units of about 30 donor or acceptor molecules. Both, the formation of an oblique mesophase and the limited miscibility between PBI and triphenylene units are probably caused by their different shape anisotropies (board-shaped vs. disc-shaped).

2.2. Perylene Tetraesters (PTE)

Kitzerow and co-workers reported the first mesomorphic 3,4,9,10-tetra-(alkoxycarbonyl)-perylene as early as in 2000,^[120–122] yet the overall number of reported liquid crystalline PTEs has remained small (Figure 16a).^[40] This class of perylene-based materials, also known as perylene tetraesters (PTEs), commonly exhibits much higher solubility than PBIs. However, their thermal stability is lower and their ester groups are susceptible to hydrolysis and transesterification. PTEs possess

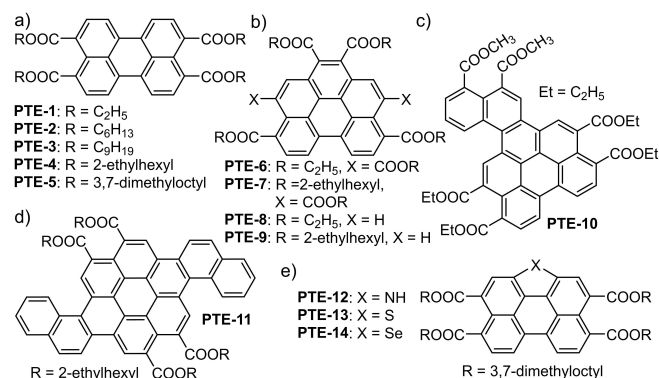


Figure 16. a) Structures of selected mesomorphic PTEs, b–d) PTEs with extended cores, and e) bay-annulated PTEs that were studied for mesomorphism.

frontier orbitals of higher energy that lower their electron affinity in comparison to their PBI counterparts^[40] and the PTE core has a lower in-plane aspect ratio (less board-shaped) than the PBI core (1.5 to 1.7, respectively) (Figure 17). The higher LUMO and HOMO levels of PTEs potentially increase open circuit voltages (VOC) in heterojunction organic solar cells compared to PBI based acceptor materials.^[123]

The homologous series of PTE-1 to PTE-3 with n-ethyl, n-hexyl, and n-nonyl alkyl chains reveals robust Col_h mesomorphism with preferential homeotropic alignment.^[120] Increasing chain length leads to lower clearing points and overall decreased the temperature ranges of the mesophases until no mesophase was observed for decyl side-chains. All three PTEs exhibit intense green fluorescence in dilute solution (475–555 nm) and a red-shifted emission (550–650 nm) with longer lifetimes for their columnar mesophases. This unique behaviour and the absence of aggregation induced quenching were explained with the formation of excimers in the mesophase. The fluorescence intensity decreases when the mesophase crystallizes indicating a distinct change in electronic interactions between PTE cores.

Clearly, the conformational flexibility of the out-of-plane ester groups and the smaller conjugated system compared to PBI significantly lower the propensity of π - π stacking for PTE

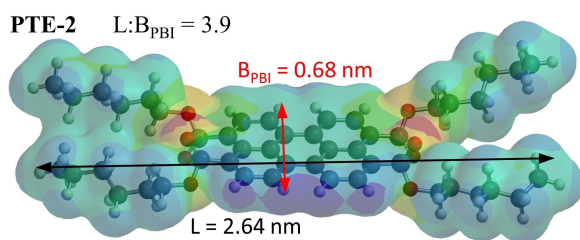


Figure 17. Electrostatic potential map projected onto density surface generated by semiempirical PM6 calculations (Spartan) for PTE-2 in the gas phase. The in-plane aspect ratio is calculated based on the estimated overall length of the molecule for side-chains in amorphous states and the breadth of the perylene core.

| Comp. | DSC transition T [°C] and (ΔH [kJ mol ⁻¹]) on heating ^[a] | Ref. |
|--------|---|-----------|
| PTE-1 | Cr 244 (3 [J g ⁻¹]) Col _h 313 (19.5 [J g ⁻¹]) I | [120,121] |
| PTE-2 | Cr 72 (58 [J g ⁻¹]) Col _h 177 (3.5 [J g ⁻¹]) I | [120,121] |
| PTE-3 | Cr 60 (28 [J g ⁻¹]) Col _h 100 (1.4 [J g ⁻¹]) I | [120,121] |
| PTE-4 | Col _h 240 I | [121] |
| PTE-5 | Col _h 150 (6.23) I | [125] |
| PTE-6 | Cr 203 (11.3) I | [126] |
| PTE-7 | Isotropic liquid at room temperature | [126] |
| PTE-8 | Cr 200 Col _h 302 (8.5) I | [126] |
| PTE-9 | Col _h 182 (9.8) I | [126] |
| PTE-10 | LC 230 I | [127] |
| PTE-11 | Cr 227.6 I | [112] |
| PTE-12 | Col _h 284.6 (33.5) I | [128] |
| PTE-13 | Col _h 199.9 (38.3) I | [128] |
| PTE-14 | Col _h 182.2 (29.7) I | [128] |

[a] All phase assignments are based on DSC analysis, defect textures obtained by POM, and XRD data.

(Figure 17). Consequently, alkyl groups are sufficient for introducing mesomorphism and only one PTE derivative with oligo(ethyleneoxy) chains has been reported.^[124] The introduction of branched side-chains 2-ethylhexyl and 3,7-dimethyloctyl stabilizes the Col_h mesophases of PTE-4 and PTE-5, respectively, in comparison to linear alkyl chains of the same number of carbon atoms and suppresses crystallization because of the generated mixtures of stereoisomers (Figure 16a and Table 4).^[121–125]

The groups of Bock^[126,127] and Kitzerow^[112] altered the chromophore's thermal and electronic properties by expanding the PTE core in one of the two bay regions to give PTE-6 to PTE-11 (Figure 16b–d). Surprisingly, hexaester PTE-6 shows only monotropic Col_h mesomorphism and PTE-7 is not mesomorph at all, but an isotropic liquid at room temperature. In contrast, the tetraesters PTE-8 and PTE-9 exhibit enhanced enantiotropic Col_h mesomorphism and the latter is liquid crystalline down to room temperature.^[126,127] This large difference in mesomorphism between tetraesters and hexaesters is reasoned with an overcrowding of alkoxy carbonyl groups that prevents close π - π stacking of neighbouring cores because of their out-of-plane orientations. Four ester groups leave enough space for staggered stacking of the cores but six do not.

Hexaester PTE-10 maintains stable columnar mesomorphism and preferentially aligns homeotropically (planar) (Figure 16c). Here, the asymmetric extension of the bay region with a dimethyl ester of naphthalene dicarboxylic acid leaves sufficient space for staggered π - π stacking. The low symmetry of the core helps with suppressing crystallization, which extends the mesophase below room temperature despite the rather short ethyl side-chains.^[127]

The more symmetric bilaterally extended PTE-11 with two naphthalene moieties at the bay-positions was not mesomorph, neither with straight (not shown) nor with branched chains (Figure 16d).^[112] This may be for two reasons: a) its melting point is very high because it crystallizes more easily, b) its aromatic core is not planar and prevents a staggered packing of the ester groups in a columnar π - π stack. Also unusual is the blue shifted absorption and emission of the compound compared to the parent PTE. This is explained by an overall reduction in conjugation for PTE-11 based on quantum chemical calculations because of its nonplanar structure and despite the formal increase in size of the aromatic core. In addition, charge-transfer effects between the outer and inner parts of the extended core generate unique absorption bands in the UV range.

Achalkumar's group explored bay-annulated PTE derivatives PTE-12 to PTE-14 with bridging heteroatoms S, Se, and NH to probe their emission properties and mesomorphism (Figure 16e).^[128–131] The N-annulated PTEs exhibit mesomorphism over the widest range of temperature, in contrast to related PBI-46 to -48 that show the widest temperature ranges and most stable Col_h mesophases for the S and Se derivatives. Incorporation of branched 3,7-dimethyloctyl chains lowers the melting points of compounds PTE-12 to PTE-14 below room temperature.

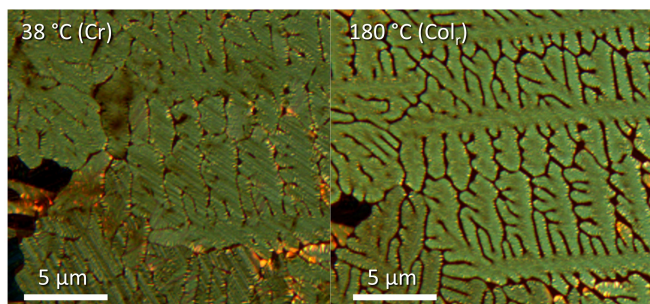


Figure 19. Defect textures of the crystalline and rectangular columnar mesophase (Col_o) of IIND-1 observed by POM.^[136] Reproduced from Ref. [136] with permission. Copyright (2019) Wiley-VCH.

4. Mesomorphic Diketopyrrolopyrrole (DPP) Dyes

Since its coincidental discovery in 1974, DPP has become a versatile commercial pigment and dye that is currently widely studied for applications as fluorophores and in organic electronics.^[32,137,138] Only little attention has been given to its potential as functional building block for mesomorphic compounds, which may have to do with its seemingly limited options for substitution with only 4 possible substitution sites. However, the four available positions are almost orthogonal to each other, which provides ample control over the overall shape of DPP derivatives and possible directional intermolecular interactions (Figure 20).

Synthetically straightforward is the differentiation between the orthogonal pairs of substituents R^{1,2} and R^{3,4}. These DPP derivatives are often referred to as symmetric DPPs because their opposite substituents are identical (R¹ = R² and R³ = R⁴). More involved is the stepwise synthesis of the DPP core^[138,139] but it provides controlled access to unsymmetric DPP derivatives with R¹ ≠ R², although, this has mostly been achieved by statistical substitution.^[140–143] In contrast, a sequential attachment of substituents R³ and R⁴ to N has not been reported and the few known DPPs with R³ ≠ R⁴ were exclusively obtained by statistical substitution and chromatographic separation of the obtained product mixtures.^[144]

Praefcke and Ciba Specialty Chemicals reported the first liquid crystalline DPP derivatives in 1998 and 1999, respectively. These DPP derivatives are elongated by substituents R¹ and R² to give overall rod-shaped structures (calamitic liquid crystals) and predominantly display nematic and smectic mesophases (Figure 20).^[145,146] The calamitic rather than board-shaped character of these compounds is also enhanced by the non-planar

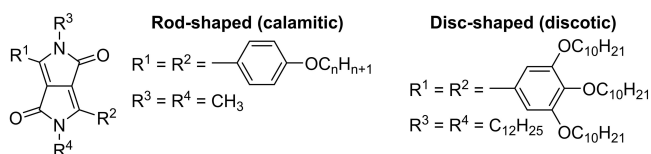


Figure 20. General substitution pattern of DPP and examples of a rod-shaped (DPP-5) and a disc-shaped (DPP-7) mesomorphic derivative.

structure of the diphenyl DPP cores. Most of these compounds were reported in a patent that provides limited information on the types of liquid crystal phases, their phase transition temperatures, and no XRD data were reported. All DPP derivatives that have been listed as nematic, smectic, and discotic columnar liquid crystals are given in Table 6.

However, the liquid crystal phases reported for some specific DPP derivatives are consistent with established molecular design criteria. Elongation along R¹ and R² and short alkyl chains as R^{3,4} generated rod-shaped DPP derivatives that display nematic mesophases with shorter alkyl groups and smectic mesophases with longer alkyl groups attached to R^{1,2} due to microphase segregation (e.g. DPP-4 in Table 6). Attachment of three alkyl chains to each R¹ and R² and longer alkyl groups as R^{3,4} generated overall more disc-shaped molecules that preferentially self-assembled into columnar stacks (e.g. DPP-7). Overall, this large body of work illustrates that DPP based liquid crystals obey the established structure property relations for calamitic and discotic liquid crystals. Although, attempts of generating liquid crystals by elongating DPP along R³ and R⁴ have not been successful.

Unfortunately, no information on the types of liquid crystal phases and their temperature ranges was provided for DPP derivatives of less usual structures, such as DPP-2, -5, and -8, that were reported to be mesomorphic. New and less conventional work on mesomorphic DPP derivatives has surfaced only recently. DPP-15, a truly board-shaped DPP derivative shown in Figure 21 was obtained by attaching diphenyltriazine groups.^[136] Here, the entire conjugated system is planar and its columnar self-assembly is not only controlled by the large number and packing volume of the overall 14 octyloxy and

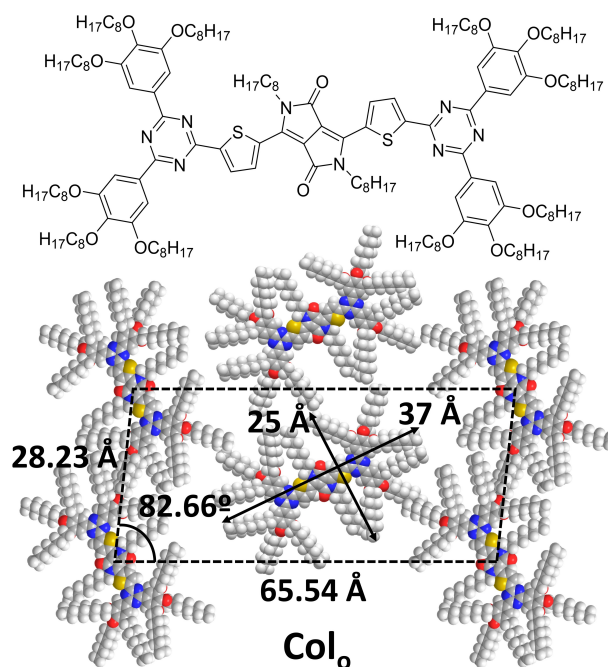
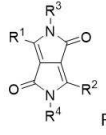
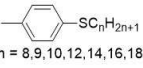
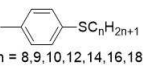
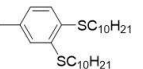
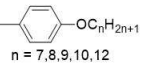
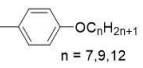
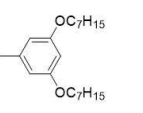
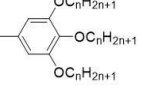
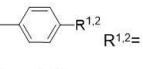
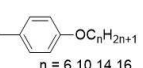
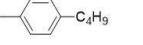
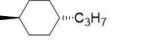
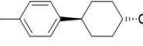
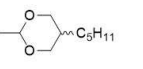


Figure 21. Molecular structure, defect texture, and proposed packing model for an oblique columnar mesophase of this board-shaped DPP derivative DPP-15.^[136] Reproduced from Ref. [136] with permission. Copyright (2019) Wiley-VCH.

Table 6. Liquid crystalline DPP derivatives reported by Praefcke and Ciba Specialty Chemicals.

| DPP-# Ref. |  R ^{1,2} for | R ^{3,4} | Liquid crystal temp. range [°C] and (ΔH [kJ mol ⁻¹]) ^[a] N = Nematic; Sm = Smectic; Col = Columnar |
|----------------------|---|--|---|
| DPP-1 [145] |  n = 8, 9, 10, 12, 14, 16, 18 | CH ₃ | n = 12: 104–114 n = 16: 90–114 phases not specified for all others |
| DPP-2 [145] |  n = 8, 9, 10, 12, 14, 16, 18 | C ₁₂ H ₂₅ for n = 8, 9 C ₁₆ H ₃₃ for n = 10 C ₁₂ H ₂₅ for n = 12 C ₁₆ H ₃₃ for n = 12 C ₁₈ H ₃₇ for n = 14, 16, 18 | mesophases not specified |
| DPP-3 [145] |  | CH ₃ | not liquid crystalline |
| DPP-4 [145, 146] |  n = 7, 8, 9, 10, 12 | CH ₃ | n = 8: 106(59) N 114(0.9) ^[b] n = 10: 106(69) SmA 119(3.0) ^[b] n = 12: 108(82) SmA 123(4.7) ^[b] |
| DPP-5 [145] |  n = 7, 9, 12 | n = 7, 9: C ₁₀ H ₂₁ n = 9, 12: C ₁₂ H ₂₅ n = 12: C ₁₆ H ₃₃ | mesophases not specified |
| DPP-6 [145] |  | C ₁₀ H ₂₁ | mesophases not specified |
| DPP-7 [145] |  | CH ₃ C ₁₂ H ₂₅ | For CH ₃ : n = 6: 117(36) Col 146 n = 8: 83(32) Col 129 n = 10: 65(45) Col 114 |
| DPP-8 [145] | R ¹ = C ₇ H ₁₅ , R ² = C ₇ H ₁₅ R ¹ = C ₆ H ₁₃ , R ² = <i>p</i> -Cl-C ₆ H ₄ R ¹ = C ₆ H ₁₃ , R ² = <i>p</i> -Cl-C ₆ H ₄ R ¹ = C ₇ H ₁₅ , R ² = <i>p</i> -Cl-C ₆ H ₄ R ¹ = C ₇ H ₁₅ , R ² = <i>p</i> -Cl-C ₆ H ₄ | C ₇ H ₁₅ CH ₃ C ₆ H ₁₃ CH ₃ C ₇ H ₁₅ | mesophases not specified |
| DPP-9 [145] |  R ¹ = O(CH ₂) ₂ OC ₂ H ₅ R ¹ = C ₁₀ H ₂₁ | R ^{3,4} | Liquid crystal range in °C (kJ/mol) |
| DPP-10 [145, 146] |  n = 6, 10, 14, 16 | CH ₃ | n = 16: 205(44) N 336(1.2) ^[b] n = 10: 139 N 303 n = 14: 137(32) Sm 280 n = 16: 116 N ^[c] 235 |
| DPP-11 [145] |  | CH ₃ | 220(4.0) N 330(0.1) ^[b] |
| DPP-12 [145, 146] |  | CH ₃ | 191(23) N 358(1.7) ^[b] |
| DPP-13 [145, 146] |  | CH ₃ C ₂ H ₅ C ₃ H ₇ | CH ₃ : 248(31) N 327(0.3) ^[b] CH ₂ CH ₃ : 243(38) N 349(0.2) ^[b] CH ₂ CH ₂ CH ₃ : 210(36) N 337 |
| DPP-14 [145] |  | CH ₃ | 182(20) N narrow range |

[a] DSC data were provided only for a few compounds reported in the patent. [b] Taken from reference Praefcke LC. [c] Likely a smectic phase.

octyl chains but also their longitudinal and lateral spatial orientations. The compound displays a rare oblique columnar mesophase between 46 °C and 222 °C that supports π - π stacking interactions between molecules. No evidence was found for specific rotation angles between stacking molecules that could, for example, result in an overall helical packing.

Rather exceptional is the columnar mesomorphism shown in Figure 22 reported for a DPP derivative with H for $R^{3,4}$ (DPP-16).^[147] Microphase segregation between the 6 dodecyloxy groups and the diphenyl DPP core could have generated conventional columnar mesomorphism with π - π stacking cores, but this would have excluded the formation of intracolumnar H-bonding interactions between lactam groups. Intercolumnar H-bonding interactions are usually disfavoured because they interfere with the typical rotational dynamics of molecules in columnar stacks.

The observed supramolecular structure includes π -stacking interactions for the formation of dimers, strong intracolumnar H-bonding interactions between dimers, and an effective space filling by the side-chains to wrap in the columnar stack of dimers. Rotation about the stacking axis was still viable although H-bonding between two dimers will be temporarily affected if a dimeric unit of a column rotates. Related H-bonded columnar mesophases were reported for compounds PBI-47 to PBI-49 described earlier.

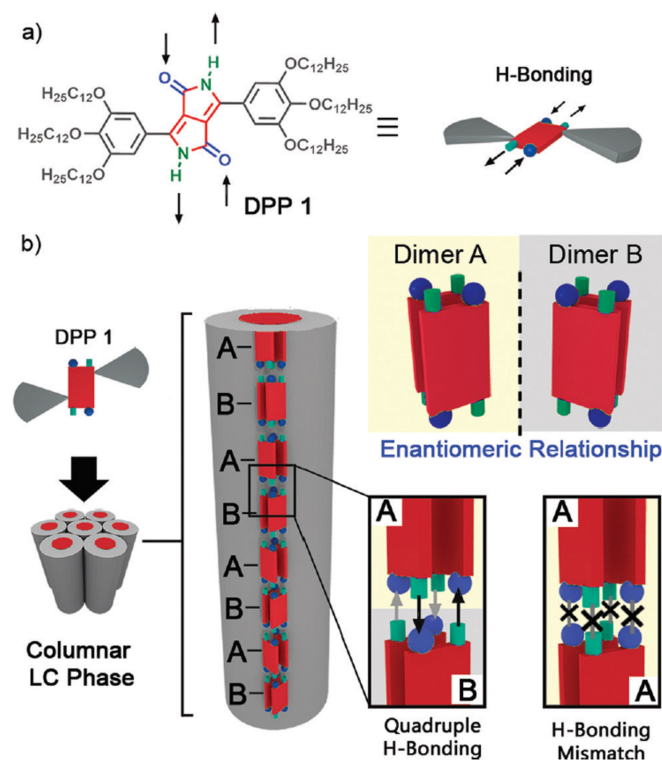


Figure 22. Proposed packing model for a columnar mesophase generated by a H-bonding DPP derivative (DPP 1 = DPP-16 here) with tridodecyloxyphenyl groups for $R^{1,2}$ and H for $R^{3,4}$. A racemate of dimers is formed by π -stacking interactions between two molecules. The two enantiomeric dimers alternatingly stack by strong intracolumnar H-bonding interactions and the dictated 90° rotation between dimers facilitates an effective space filling by the 12 side-chains per dimer.^[147] Reproduced from Ref. [147] with permission. Copyright (2017) Wiley-VCH.

A few other DPP derivatives have been reported as being liquid crystalline but the provided experimental evidence is insufficient for a definitive assignment of liquid crystal phases. Certainly, these compounds display mesophases of some sort and show interesting opto-electronic properties. Triads of two DPPs with a central hexabenzocoronene, a well-known discotic mesogen, self-assemble into columnar stacks for $Y = H$ and into lamellar mesophases for more elongated derivatives with $Y = 2$ -benzothiophene and 2-benzofuran (DPP-17 a–c in Figure 23).^[148] Derivatives DPP-18 a–b in Figure 23 rather display soft crystal mesophases than liquid crystal phases based on the provided DSC data and POM images.^[149,150]

DPP derivatives have been used as components of liquid crystalline polymers^[151,152] and as dye additives to liquid crystal matrices^[153,154] that are not further discussed here. Also outside the scope of this review are DPP derivatives that self-assemble on surfaces and at interfaces^[155,156] or show specific types of aggregation.^[157,158]

5. Mesomorphic Quinoxalinophenanthrophenazine (QPP)

Despite its relatively large size, the QPP core is readily accessible by condensations of orthodiamino benzene derivatives with tetraketo pyrrole (Figure 24). Equally favourable are its high thermal and chemical stability, absorption in the visible range, and strong fluorescence. QPP derivatives have mainly been studied as organic semiconductors^[159–165] and as an active material in optical sensors.^[166,167] In combination with triptycene, QPP has recently been reported as a versatile building block for porous crystalline materials^[168–170] and for organogelators.^[171]

While the QPP core can still be classified as a board-shaped structure, its in-plane aspect ratio of 5–6 is that of a rod-shaped (calamitic) liquid crystal (Figure 25). Such molecules are expected to have a much higher propensity for forming nematic and lamellar (smectic) mesophases rather than columnar mesophases. However, no calamitic liquid crystal phases have been observed for any of the reported mesomorphic QPPs,

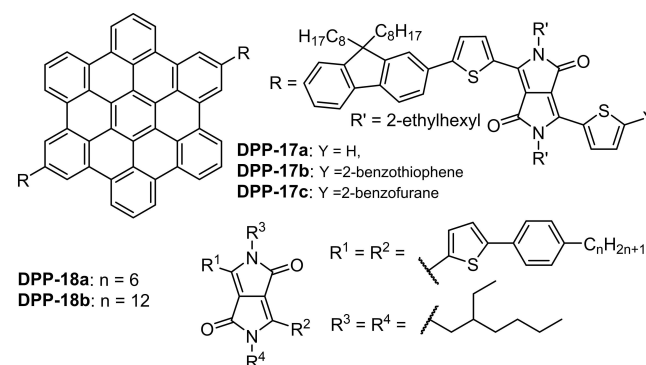


Figure 23. DPP derivatives that have been proposed to be liquid crystalline but might be better categorized as higher ordered mesophase and anisotropic glasses.

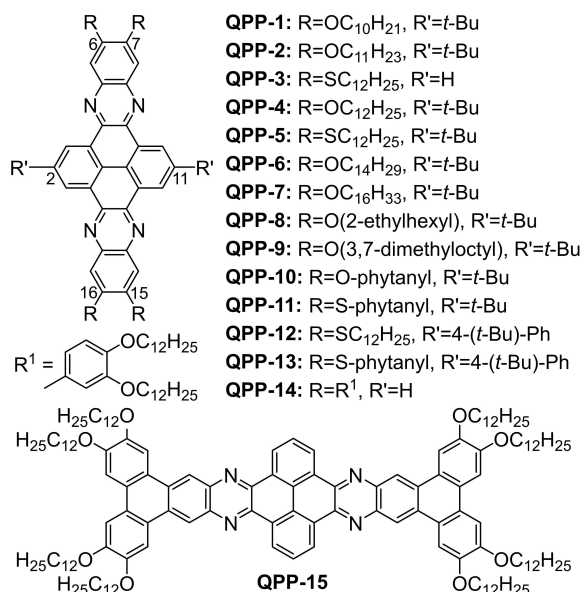


Figure 24. QPP derivatives that have been reported to be liquid crystalline and some structurally related derivatives that are not mesomorph (see Table 7).

The in-plane aspect ratio of QPP with R = SC₁₂H₂₅ decreases from an estimated value of 5.4 for R' = H to 4.7 for R' = t-Bu and 2.6 for R'=4-(t-Bu)-Ph.

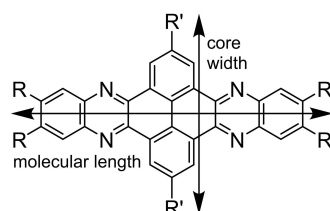


Figure 25. Estimated in-plane aspect ratios for QPP cores with different R' groups in 2 and 11 positions.

although zone-casted thin films of **QPP-4** display highly ordered lamellar phases.^[161]

QPP derivatives with H or t-Bu groups in 2 and 11 positions and four linear alkoxy groups attached to positions 6, 7, 15, and 16 showed complex polymorphism of their crystalline phases. The high temperature phases of derivatives **QPP-1** and **-2** with C₁₀ and C₁₁ chains, respectively, are tentatively assigned as liquid crystal phases but more likely represent disordered crystal phases with 3-dimensional positional order (Table 7).^[172,173] Certainly, the provided DSC, POM, and XRD data are more consistent with the latter. Derivatives with shorter alkyl chains than nine carbons melt well above 300 °C, where thermal stability is compromised.^[173] Derivatives with longer linear alkyl chains than eleven carbons and branched side-chains (**QPP-4,6-9**) do not display mesophases although their melting points decrease with increasing length of their linear chains. Surprisingly, incorporation of branched 2-ethylhexyloxy and 3,7-dimethyloctyloxy chains in **QPP-8** and **-9** increases melting points above 300 °C,^[172] which is rather unusual for chains with branching points close to a core. Branching at the end of alkyl chains has been shown to increase melting points of some discotic liquid crystals, presumably because of better space filling of the side-chain continuum.^[175]

Table 7. Phase transition temperatures and enthalpies for QPP derivatives shown in Figure 24. Cr = crystal, M = mesophase of unknown structure; Col = columnar mesophase of unknown structure; Col_h or _r = columnar mesophase of hexagonal or rectangular structure, respectively; I = isotropic liquid, Dec = decomposition.

| Comp. | DSC transition <i>T</i> [°C] and [Δ <i>H</i> [kJ mol ⁻¹]] on heating | Ref. |
|---------------|---|-----------|
| QPP-1 | Cr 213 (36.2) LC 268 (12.5) I ^[a] | [172,173] |
| QPP-2 | Cr 210 (n.a.) LC 234 (n.a.) I ^[a] | [172,173] |
| QPP-3 | Cr 167 (52.8) I | [37] |
| QPP-4 | Cr 211 (n.a.) I | [37,174] |
| QPP-5 | Cr ₁ 96 (2.4) Cr ₂ 271 (44.5) I | [37,174] |
| QPP-6 | Cr 202 (n.a.) I | [172,173] |
| QPP-7 | Cr 178 (n.a.) I | [173] |
| QPP-8 | Cr > 350 (n.a.) I/Dec ^[b] | [172] |
| QPP-9 | Cr 316 (n.a.) I | [172] |
| QPP-10 | M 126 (12.9) Col _r 152 (3.1) I | [37,173] |
| QPP-11 | Cr 142 (30.6) I | [37] |
| QPP-12 | Cr ₁ 29 (2.2) Cr ₂ 204 (50.7) Col _h 349 (4.4) I/Dec ^[b] | [37] |
| QPP-13 | Cr 105 (19.5) Col _h 239 (<0.5) I | [37] |
| QPP-14 | Cr 33 (52.1) Col _r 91 (12.8) Col _h 159 (<0.1) I | [36] |
| QPP-15 | Cr 123 (206) Col > 263 Dec | [36] |

[a] Both compounds display crystalline polymorphism and whether the highest temperature phase is liquid crystalline remains uncertain (see text for details). [b] Decomposition coincides with phase transition.

In contrast, attachment of multiple branched phytanyloxy chains (2,6,10,14-tetramethylhexadecyloxy) significantly reduces the melting point of **QPP-10** and induces columnar mesomorphism over a small temperature range of 26 °C. The lateral packing volume of this side-chain is apparently sufficient for effectively filling the peripheral space of a tilted columnar stack. However, thioether analogue **QPP-11** was not mesomorph even though the melting point of **QPP-11** was below the clearing point of **QPP-10**.

Compounds **QPP-1** to **-11** have in-plane aspect ratios larger than 4 that usually promote lamellar over columnar mesomorphism, especially if the lateral packing volume of the side-chains does not significantly exceed that of the core (Figure 25).

Columnar mesomorphism over a wide range of temperatures is achieved by either reducing the in-plane aspect ratio of the core or by increasing the lateral packing volume of the side-chains. Attachment of 4-*tert*-butylphenyl groups to positions 2 and 11 (**QPP-12**, **-13**) generates crucifix-shaped compounds with in-plane aspect ratios of smaller than 3.^[37] This is sufficient for stabilizing hexagonal columnar mesophases over a wide range of temperatures and with high thermal stability (at least 350 °C for **QPP-12**).

Attachment of 3,4-didodecyloxyphenyl groups to positions 6, 7, 15, and 16 in compounds **QPP-14** and **-15** reduced the in-plane aspect ratio by significantly increasing the lateral packing volume of the side-chains at each end of the long axis of the core (Figure 25).^[36] This reduction in aspect ratio is achieved by the incorporation of 4 side-chains on each side (octacatenar) and their spatial orientation not only along but also orthogonal to the long axis of the molecule (dumbbell-shape). **QPP-14** crystallizes from its rectangular columnar mesophase just above room temperature, which is astonishing for such a large molecule and this is attributed to the non-planar phenyl groups. Oxidative coupling of the phenyl groups to planar

triphenylene end groups of the core in QPP-15 increases both, the melting point and the thermal stability of the hexagonal columnar mesophase by about 100 °C.

6. Summary and Outlook

Columnar mesomorphism has been reported for all reviewed board-shaped dyes perylene bisimide, perylene tetracarboxylic ester, indigo, isoindigo, diketopyrrolopyrrole, and quinoxalino-phenanthrophenazine and was exclusively achieved by the appropriate attachment of flexible side-chains of sufficient overall and lateral packing volume. Columnar mesophases of perylene bisimides (PBIs) have been studied most widely and detailed investigations revealed packing structures in which the long axis of the PBI core rotates about the stacking axis. In some cases, the rotation angle was consistent over many repeat units to generate helical stacks. These packing structures explain how molecules with calamitic like aspect ratios of > 5 self-organize into columnar stacks and provide instructive examples for how to minimize aggregation caused quenching of fluorescence while maintaining π - π stacking. Their overall structure and underlying molecular dynamics are distinctly different from columnar mesophases of typical discotic liquid crystals.

Rather unusual columnar mesomorphism that does not rely on long π - π stacks was achieved with perylene bisimide and diketopyrrolopyrrole derivatives by utilizing their strong and directional H-bonding interactions. Here, H-bonding between imide and lactam groups orients the long axis of the molecules parallel to the column axis to generate strands of H-bonded molecules and several strands form a columnar unit.

Despite the large structural diversity at the molecular and supramolecular level, designing one type of molecule that satisfies all required materials properties remains a challenge. More fruitful may be the use of mixtures of compounds and, in our opinion, columnar mesophases of board-shaped dyes provide some unique opportunities in this regard.

Acknowledgements

The authors thank Kaila Wilson and Julia Cordeiro for their artistic work on Figures 1 (J.C.) and 3 (J.C. and K.W.) and the frontispiece (K.W.). S.H.E. acknowledges funding from NSERC (RGPIN-2019-07271). B. R. K. thanks the University Research Board (URB) of the American University of Beirut and the Lebanese National Council for Scientific Research (CNRS) for financial support.

Conflict of Interest

The authors declare no conflict of interest.

Keywords: board-shaped dyes · columnar mesomorphism · liquid crystals · mesophases · self-assembly

- [1] *Supramolecular Dye Chemistry* (Ed.: F. Würthner), Springer-Verlag, Berlin, Heidelberg, 2005.
- [2] F. Würthner, T. E. Kaiser, C. R. Saha-Möller, *Angew. Chem. Int. Ed.* **2011**, *50*, 3376–3410; *Angew. Chem.* **2011**, *123*, 3436–3473.
- [3] J. Bernstein, in *Polymorphism in Molecular Crystals*, Oxford University Press, Oxford, **2002**, p. 257.
- [4] L. Dähne, E. Biller, *Adv. Mater.* **1998**, *10*, 241–245.
- [5] Y. Ji, Z. Peng, B. Tong, J. Shi, J. Zhi, Y. Dong, *Dyes Pigm.* **2017**, *139*, 664–671.
- [6] K. Naito, Y. Watanabe, S. SyunEgusa, *Jpn. J. Appl. Phys.* **1999**, *38*, 2792.
- [7] Z. Chen, U. Baumeister, C. Tschierske, F. Würthner, *Chem. Eur. J.* **2007**, *13*, 450–465.
- [8] B. R. Kaafarani, *Chem. Mater.* **2011**, *23*, 378–396.
- [9] Y. Zhang, H. Wang, Y. Xiao, L. Wang, D. Shi, C. Cheng, *ACS Appl. Mater. Interfaces* **2013**, *5*, 11093–11100.
- [10] S. Sergeev, W. Pisula, Y. H. Geerts, *Chem. Soc. Rev.* **2007**, *36*, 1902–1929.
- [11] S. Laschat, A. Baro, N. Steinke, F. Giesselmann, C. Hägele, G. Scalia, R. Judele, E. Kapatsina, S. Sauer, A. Schreivogel, M. Tosoni, *Angew. Chem. Int. Ed.* **2007**, *46*, 4832–4887; *Angew. Chem.* **2007**, *119*, 4916–4973.
- [12] C. Tschierske, in *Handbook of Liquid Crystals*, Wiley-VCH, Weinheim, **2014**, pp. 1–44.
- [13] C. Tschierske, in *Handbook of Liquid Crystals*, Wiley-VCH, Weinheim, **2014**, pp. 45–88.
- [14] J. W. Goodby, P. J. Collings, T. Kato, C. Tschierske, H. F. Gleeson, P. Raynes, Eds., *Handbook of Liquid Crystals*, Wiley-VCH Verlag GmbH, **2014**.
- [15] C. Tschierske, *Angew. Chem. Int. Ed.* **2013**, *52*, 8828–8878; *Angew. Chem.* **2013**, *125*, 8992–9047.
- [16] S. Mairie, D. Haristoy, J.-F. Nicoud, D. Guillon, S. Diele, H. Monobe, Y. Shimizu, *J. Mater. Chem.* **2002**, *12*, 37–41.
- [17] M. Ebert, R. Kleppinger, M. Soliman, M. Wolf, J. H. Wendorff, G. Lattermann, G. Stauffer, *Liq. Cryst.* **1990**, *7*, 553.
- [18] G. R. Luckhurst, *Thin Solid Films* **2001**, *393*, 40–52.
- [19] J. P. Straley, *Phys. Rev. A* **1974**, *10*, 1881–1887.
- [20] M. Lehmann, S. Maisch, N. Scheuring, J. Carvalho, C. Cruz, P. J. Sebastião, R. Y. Dong, *Soft Matter* **2019**, *15*, 8496–8511.
- [21] H. Huang, Y. Huang, S. Wang, M. Zh, H. Xie, L. Zhang, X. Zheng, Q. Xie, D. Niu, Y. Gao, *Crystals* **2016**, *6*, DOI 10.3390/cryst6090113.
- [22] T. Weil, T. Vosch, J. Hofkens, K. Peneva, K. Müllen, *Angew. Chem. Int. Ed.* **2010**, *49*, 9068–9093; *Angew. Chem.* **2010**, *122*, 9252–9278.
- [23] F. Würthner, C. R. Saha-Möller, B. Fimmel, S. Ogi, P. Leowanawat, D. Schmidt, *Chem. Rev.* **2016**, *116*, 962–1052.
- [24] S. Chen, P. Slattum, C. Wang, L. Zang, *Chem. Rev.* **2015**, *115*, 11967–11998.
- [25] V. Vohra, *Materials* **2018**, *11*, 2579.
- [26] M. Irimia-Vladu, Y. Kanbur, F. Camaioni, M. E. Coppola, C. Yumusak, C. V. Irimia, A. Vlad, A. Operamolla, G. M. Farinola, G. P. Suranna, N. González-Benitez, M. C. Molina, L. F. Bautista, H. Langhals, B. Stadlober, E. D. Glowacki, N. S. Sariciftci, *Chem. Mater.* **2019**, *31*, 6315–6346.
- [27] N. M. Randell, T. L. Kelly, *Chem. Rec.* **2019**, *19*, 973–988.
- [28] S. M. McAfee, G. C. Welch, *Chem. Rec.* **2019**, *19*, 989–1007.
- [29] J.-L. Li, J.-J. Cao, L.-L. Duan, H.-L. Zhang, *Asian J. Org. Chem.* **2018**, *7*, 2147–2160.
- [30] D. Xia, C. Li, W. Li, *Chem. Rec.* **2019**, *19*, 962–972.
- [31] A. Venkateswararao, S.-W. Liu, K.-T. Wong, *Mat. Sci. Eng.* **2018**, *124*, 1–57.
- [32] A. Tang, C. Zhan, J. Yao, E. Zhou, *Adv. Mater.* **2017**, *29*, 1600013.
- [33] Y. Patil, R. Misra, *Chem. Asian J.* **2018**, *13*, 220–229.
- [34] Y. Patil, R. Misra, *J. Mater. Chem. C* **2019**, *7*, 13020–13031.
- [35] W. Li, L. Wang, H. Tang, D. Cao, *Dyes Pigm.* **2019**, *162*, 934–950.
- [36] S. Chen, F. S. Raad, M. Ahmida, B. R. Kaafarani, S. H. Eichhorn, *Org. Lett.* **2013**, *15*, 558–561.
- [37] A. O. El-Ballouli, H. Kayal, C. Shuai, T. A. Zeidan, F. S. Raad, S. Leng, B. Wex, S. Z. D. Cheng, S. H. Eichhorn, B. R. Kaafarani, *Tetrahedron* **2015**, *71*, 308–314.
- [38] F. Würthner, C. R. Saha-Möller, B. Fimmel, S. Ogi, P. Leowanawat, D. Schmidt, *Chem. Rev.* **2016**, *116*, 962–1052.
- [39] S. Laschat, A. Baro, N. Steinke, F. Giesselmann, C. Hägele, G. Scalia, R. Judele, E. Kapatsina, S. Sauer, A. Schreivogel, M. Tosoni, *Angew. Chem. Int. Ed.* **2007**, *46*, 4832–4887; *Angew. Chem.* **2007**, *119*, 4916–4973.
- [40] R. K. Gupta, A. A. Sudhakar, *Langmuir* **2019**, *35*, 2455–2479.
- [41] M. M. Elmahdy, X. Dou, M. Mondeshki, G. Floudas, H.-J. Butt, H. W. Spiess, K. Müllen, *J. Am. Chem. Soc.* **2008**, *130*, 5311–5319.

- [42] X. Shen, R. Y. Dong, N. Boden, R. J. Bushby, P. S. Martin, A. Wood, *J. Chem. Phys.* **1998**, *108*, 4324–4332.
- [43] M. R. Hansen, X. Feng, V. Macho, K. Müllen, H. W. Spiess, G. Floudas, *Phys. Rev. Lett.* **2011**, *107*, 257801.
- [44] M. R. Hansen, T. Schnitzler, W. Pisula, R. Graf, K. Müllen, H. W. Spiess, *Angew. Chem. Int. Ed.* **2009**, *48*, 4621–4624; *Angew. Chem.* **2009**, *121*, 4691–4695.
- [45] L. K. Hiscock, B. M. Raycraft, M. Wałęsa-Chorab, C. Cambe, A. Malinge, W. G. Skene, H. Taing, S. H. Eichhorn, L. N. Dawe, K. E. Maly, *Chem. Eur. J.* **2018**, *25*, 1018–1028.
- [46] Z. Chen, V. Stepanenko, V. Dehm, P. Prins, L. D. A. Siebbeles, J. Seibt, P. Marquetand, V. Engel, F. Würthner, *Chem. Eur. J.* **2007**, *13*, 436–449.
- [47] C. R. Newman, C. D. Frisbie, D. A. da Silva Filho, J.-L. Brédas, P. C. Ewbank, K. R. Mann, *Chem. Mater.* **2004**, *16*, 4436–4451.
- [48] B. Xu, X. Xiao, X. Yang, L. Zang, N. Tao, *J. Am. Chem. Soc.* **2005**, *127*, 2386–2387.
- [49] A. Datar, R. Oitker, L. Zang, *Chem. Commun.* **2006**, *0*, 1649–1651.
- [50] F. Würthner, C. Thalacker, A. Sautter, *Adv. Mater.* **1999**, *11*, 754–758.
- [51] L. Zang, R. Liu, M. W. Holman, K. T. Nguyen, D. M. Adams, *J. Am. Chem. Soc.* **2002**, *124*, 10640–10641.
- [52] F. Würthner, *Chem. Commun.* **2004**, *0*, 1564–1579.
- [53] C. Huang, S. Barlow, S. R. Marder, *J. Org. Chem.* **2011**, *76*, 2386–2407.
- [54] C. Li, H. Wonneberger, *Adv. Mater.* **2012**, *24*, 613–636.
- [55] C. Liu, C. Xiao, Y. Li, W. Hu, Z. Li, Z. Wang, *Chem. Commun.* **2014**, *50*, 12462–12464.
- [56] H. Wang, L. Chen, Y. Xiao, *J. Mater. Chem. C* **2017**, *5*, 12816–12824.
- [57] J. Mizuguchi, K. Tojo, *J. Phys. Chem. B* **2002**, *106*, 767–772.
- [58] W. E. Ford, *J. Photochem.* **1987**, *37*, 189–204.
- [59] W. Wang, L. S. Li, G. Helms, H. H. Zhou, A. D. Li, *J. Am. Chem. Soc.* **2003**, *125*, 1120–1121.
- [60] Z. Chen, B. Fimmel, F. Würthner, *Org. Biomol. Chem.* **2012**, *10*, 5845–5855.
- [61] X. Wang, T. Zeng, M. Nourrein, B.-H. Lai, K. Shen, C.-L. Wang, B. Sun, M. Zhu, *RSC Adv.* **2017**, *7*, 26074.
- [62] X. Zhang, Z. Chen, F. Würthner, *J. Am. Chem. Soc.* **2007**, *129*, 4886–7.
- [63] F. Zhang, Y. Ma, Y. Chi, H. Yu, Y. Li, T. Jiang, X. Wei, J. Shi, *Sci. Rep.* **2018**, *8*, 8208.
- [64] Q. Zhao, S. Zhang, Y. Liu, J. Mei, S. Chen, P. Lu, A. Qin, Y. Ma, J. Z. Sun, B. Z. Tang, *J. Mater. Chem.* **2012**, *22*, 7387–7394.
- [65] F. J. M. Hoeben, P. Jonkhøj, E. W. Meijer, A. P. H. J. Schenning, *Chem. Rev.* **2005**, *105*, 1491–1546.
- [66] K. Balakrishnan, A. Datar, T. Naddo, J. Huang, R. Oitker, M. Yen, J. Zhao, L. Zang, *J. Am. Chem. Soc.* **2006**, *128*, 7390–7398.
- [67] M.-A. Muth, G. Gupta, A. Wicklein, M. Carrasco-Orozco, T. Thurn-Albrecht, M. Thelakktat, *J. Phys. Chem. C* **2014**, *118*, 92–102.
- [68] R. A. Cormier, B. A. Gregg, *J. Phys. Chem. B* **1997**, *101*, 11004–11006.
- [69] R. A. Cormier, B. A. Gregg, *Chem. Mater.* **1998**, *10*, 1309–1319.
- [70] B. A. Gregg, R. A. Cormier, *J. Am. Chem. Soc.* **2001**, *123*, 7959–7960.
- [71] S.-G. Liu, G. Sui, R. A. Cormier, R. M. Leblanc, B. A. Gregg, *J. Phys. Chem. B* **2002**, *106*, 1307–1315.
- [72] C. Tschierske, *Isr. J. Chem.* **2012**, *52*, 935–959.
- [73] A. Wicklein, A. Lang, M. Muth, M. Thelakktat, *J. Am. Chem. Soc.* **2009**, *131*, 14442–14453.
- [74] F. May, V. Marcon, M. R. Hansen, F. Grozema, D. Andrienko, *J. Mater. Chem.* **2011**, *21*, 9538.
- [75] C. W. Struijk, A. B. Sieval, J. E. J. Dakhorst, M. van Dijk, P. Kimkes, R. B. M. Koehorst, H. Donker, T. J. Schaafsma, S. J. Picken, A. M. van de Craats, J. M. Warman, H. Zuilhof, E. J. R. Sudholter, *J. Am. Chem. Soc.* **2000**, *122*, 11057–11066.
- [76] D. M. Pereira de Oliveira Santos, M. G. Belarmino Cabral, A. Bentaleb, R. Cristiano, H. Gallardo, F. Durola, H. Bock, *Chem. Eur. J.* **2016**, *22*, 7389–7393.
- [77] F. Würthner, C. Thalacker, S. Diele, C. Tschierske, *Chem. Eur. J.* **2001**, *7*, 2245–2253.
- [78] E. O. Arikainen, N. Boden, R. J. Bushby, O. R. Lozman, J. G. Vinter, A. Wood, *Angew. Chem. Int. Ed.* **2000**, *39*, 2333–2336; *Angew. Chem.* **2000**, *112*, 2423–2426.
- [79] J. van Herrikhuysen, A. Syamakumari, A. P. Schenning, E. W. Meijer, *J. Am. Chem. Soc.* **2004**, *126*, 10021–10027.
- [80] M. Funahashi, A. Sonoda, *J. Mater. Chem.* **2012**, *22*, 25190–25197.
- [81] M. Funahashi, A. Sonoda, *Org. Electron.* **2012**, *13*, 1633–1640.
- [82] M. Funahashi, M. Yamaoka, K. Takenami, A. Sonoda, *J. Mater. Chem. C* **2013**, *1*, 7872–7878.
- [83] M. Funahashi, A. Sonoda, *Dalton Trans.* **2013**, *42*, 15987–15994.
- [84] Y. Xu, S. Leng, C. Xue, R. Sun, J. Pan, J. Ford, S. Jin, *Angew. Chem. Int. Ed.* **2007**, *46*, 3896–3899; *Angew. Chem.* **2007**, *119*, 3970–3973.
- [85] B. Gao, D. Xia, L. Zhang, Q. Bai, L. Bai, T. Yang, X. Ba, *J. Mater. Chem.* **2011**, *21*, 15975–15980.
- [86] J. Brebels, E. Douvogianni, D. Devisscher, R. Thiruvallur Eachambadi, J. Manca, L. Lutsen, D. Vanderzande, J. C. Hummelen, W. Maes, *J. Mater. Chem. C* **2018**, *6*, 500–511.
- [87] B. Meng, J. Liu, L. Wang, *Polym. Chem.* **2020**, *11*, 1261–1270.
- [88] K. Takenami, S. Uemura, M. Funahashi, *RSC Adv.* **2016**, *6*, 5474–5484.
- [89] A. Demenev, S. H. Eichhorn, T. Taerum, D. F. Perepichka, S. Patwardhan, F. C. Grozema, L. D. A. Siebbeles, R. Klenkler, *Chem. Mater.* **2010**, *22*, 1420–1428.
- [90] M. G. Debije, Z. Chen, J. Piris, R. B. Neder, M. M. Watson, K. Müllen, F. Würthner, *J. Mater. Chem. C* **2005**, *15*, 1270–1276.
- [91] Z. J. Chen, M. G. Debije, T. Debaerdemaeker, P. Osswald, F. Würthner, *ChemPhysChem* **2004**, *5*, 137–140.
- [92] V. Dehm, Z. Chen, U. Baumeister, P. Prins, L. D. A. Siebbeles, F. Würthner, *Org. Lett.* **2007**, *9*, 1085–1088.
- [93] J. F. van der Pol, E. Neeleman, J. W. Zwikker, W. Drenth, R. J. M. Nolte, *Recl. Trav. Chim. Pays-Bas* **1988**, *107*, 615–620.
- [94] V. Percec, M. Peterca, T. Tadjiev, X. Zeng, G. Ungar, P. Leowanawat, E. Aqad, M. R. Imam, B. M. Rosen, U. Akbey, R. Graf, S. Sekharan, D. Sebastiani, H. W. Spiess, P. A. Heiney, S. D. Hudson, *J. Am. Chem. Soc.* **2011**, *133*, 12197–12219.
- [95] D. Sahoo, M. Peterca, E. Aqad, B. E. Partridge, P. A. Heiney, R. Graf, H. W. Spiess, X. Zeng, V. Percec, *J. Am. Chem. Soc.* **2016**, *138*, 14798–14807.
- [96] B. Jancy, S. K. Asha, *Chem. Mater.* **2008**, *20*, 169–181.
- [97] M. Zhu, Y. Chen, H. Guo, F. Yang, X. Song, *New J. Chem.* **2018**, *42*, 8998–9005.
- [98] R. K. Gupta, D. S. Shankar Rao, S. K. Prasad, A. S. Achalkumar, *Chem. Eur. J.* **2018**, *24*, 3566–3575.
- [99] G. A. Bhavsar, S. K. Asha, *Chem. Eur. J.* **2011**, *17*, 12646–12658.
- [100] K. P. Prajitha, S. Chithiravel, K. Krishnamoorthy, S. K. Asha, *J. Mater. Chem. C* **2014**, *2*, 9882.
- [101] V. Percec, S. D. Hudson, M. Peterca, P. Leowanawat, E. Aqad, R. Graf, H. W. Spiess, X. Zeng, G. Ungar, P. A. Heiney, *J. Am. Chem. Soc.* **2011**, *133*, 18479–18494.
- [102] V. Percec, H. J. Sun, P. Leowanawat, M. Peterca, R. Graf, H. W. Spiess, X. Zeng, G. Ungar, P. A. Heiney, *J. Am. Chem. Soc.* **2013**, *135*, 4129–4148.
- [103] S. Herbst, B. Soberats, P. Leowanawat, M. Stolte, M. Lehmann, F. Würthner, *Nat. Commun.* **2018**, *9*, 2646.
- [104] S. Herbst, B. Soberats, P. Leowanawat, M. Lehmann, F. Würthner, *Angew. Chem. Int. Ed.* **2017**, *56*, 2162–2165; *Angew. Chem.* **2017**, *129*, 2194–2197.
- [105] M. Hecht, T. Schlossarek, M. Stolte, M. Lehmann, F. Würthner, *Angew. Chem. Int. Ed.* **2019**, *58*, 12979–12983.
- [106] F. Nolde, W. Pisula, S. Müller, C. Kohl, K. Müllen, *Chem. Mater.* **2006**, *18*, 3715–3725.
- [107] K. P. Prajitha, S. K. Asha, *New J. Chem.* **2016**, *40*, 8471–8478.
- [108] M. Zhu, H. Guo, F. Yang, Z. Wang, *RSC Adv.* **2017**, *7*, 4320.
- [109] S. Chen, B. Hong, H. Guo, F. Yang, *Liq. Cryst.* **2018**, *45*, 793–800.
- [110] Y. Xiao, X. Su, L. Sosa-Vargas, E. Lacaze, B. Heinrich, B. Donnio, D. Kreher, F. Mathevet, A.-J. Attias, *CrystEngComm* **2016**, *18*, 4787–4798.
- [111] Z. An, J. Yu, B. Domercq, S. C. Jones, S. Barlow, B. Kippelen, S. R. Marder, *J. Mater. Chem.* **2009**, *19*, 6688–6698.
- [112] J. Vollbrecht, H. Bock, C. Wiebeler, S. Schumacher, H. Kitzerow, *Chem. Eur. J.* **2014**, *20*, 12026–12031.
- [113] M. Ferreira, T. S. Moreira, R. Cristiano, H. Gallardo, A. Bentaleb, P. Dechambenoit, E. A. Hillard, F. Durola, H. Bock, *Chem. Eur. J.* **2018**, *24*, 2214–2223.
- [114] M. G. Belarmino Cabral, D. M. Pereira de Oliveira Santos, R. Cristiano, H. Gallardo, A. Bentaleb, E. A. Hillard, F. Durola, H. Bock, *ChemPlusChem* **2017**, *82*, 342–346.
- [115] C. T. Imrie, in *Liquid Crystals II* (Ed.: D. M. P. Mingos), Springer, Berlin, Heidelberg, **1999**, pp. 149–192.
- [116] R. J. Mandle, M. P. Stevens, J. W. Goodby, *Liq. Cryst.* **2017**, *44*, 1–14.
- [117] K. J. Lee, J. H. Woo, Y. Xiao, E. Kim, L. M. Mazur, D. Kreher, A.-J. Attias, K. Matczyszyn, M. Samoc, B. Heinrich, S. Méry, F. Fages, L. Mager, A. D'Aléo, J. W. Wu, F. Mathevet, P. André, J.-C. Ribierre, *RSC Adv.* **2016**, *6*, 57811.
- [118] X. Kong, Z. He, Y. Zhang, L. Mu, C. Liang, B. Chen, X. Jing, A. N. Cammidge, *Org. Lett.* **2011**, *13*, 764–767.
- [119] X. Kong, H. Gong, P. Liu, W. Yao, Z. Liu, G. Wang, S. Zhang, Z. He, *New J. Chem.* **2018**, *42*, 3211–3221.

- [120] S. Benning, H.-S. Kitzerow, H. Bock, M.-F. Achard, *Liq. Cryst.* **2000**, *27*, 901–906.
- [121] T. Hassheider, S. A. Benning, H.-S. Kitzerow, M.-F. Achard, H. Bock, *Angew. Chem. Int. Ed.* **2001**, *40*, 2060–2063; *Angew. Chem.* **2001**, *113*, 2119–2122.
- [122] I. Seguy, P. Jolinat, P. Destruel, J. Farenc, R. Mamy, H. Bock, J. Ip, T. P. Nguyen, *J. Appl. Phys.* **2001**, *89*, 5442–5448.
- [123] Y. Jiang, L. Lu, M. Yang, C. Zhan, Z. Xie, F. Verpoort, S. Xiao, *Polym. Chem.* **2013**, *4*, 5612–5620.
- [124] O. Thiebaut, H. Bock, E. Grelet, *J. Am. Chem. Soc.* **2010**, *132*, 6886–6887.
- [125] S. K. Gupta, S. Setia, S. Sidiq, M. Gupta, S. Kumar, S. K. Pal, *RSC Adv.* **2013**, *3*, 12060–12065.
- [126] J. Kelber, M. F. Achard, B. Garreau-de Bonneval, H. Bock, *Chem. Eur. J.* **2011**, *17*, 8145–8155.
- [127] J. Kelber, M. F. Achard, F. Durola, H. Bock, *Angew. Chem. Int. Ed.* **2012**, *51*, 5200–5203; *Angew. Chem.* **2012**, *124*, 5290–5293.
- [128] R. K. Gupta, D. Das, M. Gupta, S. K. Pal, P. K. Iyer, A. S. Achalkumar, *J. Mater. Chem. C* **2017**, *5*, 1767–1781.
- [129] R. K. Gupta, S. K. Pathak, B. Pradhan, D. S. Shankar Rao, S. Krishna Prasad, A. S. Achalkumar, *Soft Matter* **2015**, *11*, 3629–3636.
- [130] R. K. Gupta, B. Pradhan, S. K. Pathak, M. Gupta, S. K. Pal, A. A. Sudhakar, *Langmuir* **2015**, *31*, 8092–8100.
- [131] R. K. Gupta, S. K. Pathak, B. Pradhan, M. Gupta, S. K. Pal, A. A. Sudhakar, *ChemPhysChem* **2016**, *17*, 859–872.
- [132] A. Wicklein, M.-A. Muth, M. Thelakkat, *J. Mater. Chem.* **2010**, *20*, 8646–8652.
- [133] J. Kelber, H. Bock, O. Thiebaut, E. Grelet, H. Langhals, *Eur. J. Org. Chem.* **2011**, *2011*, 707–712.
- [134] J. H. Porada, D. Blunk, *J. Mater. Chem.* **2010**, *20*, 2956.
- [135] J. H. Porada, J.-M. Neudörfl, D. Blunk, *New J. Chem.* **2015**, *39*, 8291–8301.
- [136] H. Taing, A. M. Cassar, M. U. Ocheje, S. Rondeau-Gagné, T. H. El-Assaad, C. A. Sharabati, B. R. Kaafarani, S. H. Eichhorn, *ChemPlusChem* **2019**, *84*, 103–106.
- [137] O. Wallquist, R. Lenz, *Macromol. Symp.* **2002**, *187*, 617–629.
- [138] M. Grzybowski, D. T. Gryko, *Adv. Opt. Mater.* **2015**, *3*, 280–320.
- [139] C. J. H. Morton, R. Gilmour, D. M. Smith, P. Lightfoot, A. M. Z. Slawin, E. J. MacLean, *Tetrahedron* **2002**, *58*, 5547–5565.
- [140] A.-J. Payne, S. Li, S. V. Dayneko, C. Risko, G. C. Welch, *Chem. Commun.* **2017**, *53*, 10168–10171.
- [141] J. Areephong, A. D. Hendsbee, G. C. Welch, *New J. Chem.* **2015**, *39*, 6714–6717.
- [142] D. Bharath, S. Chithiravel, M. Sasikumar, N. R. Cherreddy, B. Shanigaram, K. Bhanuprakash, K. Krishnamoorthy, V. J. Rao, *RSC Adv.* **2015**, *5*, 94859–94865.
- [143] Y. Patil, T. Jadhav, B. Dhokale, R. Misra, *Eur. J. Org. Chem.* **2016**, *2016*, 733–738.
- [144] M. Castelaín, H. Salavagione, J. L. Segura, *Org. Lett.* **2012**, *14*, 2798–2801.
- [145] Z. Hao, A. Iqbal, N. Tebaldi, K. Praefcke, *Liquid Crystalline Diketopyrrolopyrroles*, **1999**, *5*, 969, 154.
- [146] K. Praefcke, M. Jachmann, D. Blunk, M. Horn, *Liq. Cryst.* **1998**, *24*, 153–156.
- [147] B. Soberats, M. Hecht, F. Würthner, *Angew. Chem. Int. Ed.* **2017**, *56*, 10771–10774; *Angew. Chem.* **2017**, *129*, 10911–10914.
- [148] W. W. H. Wong, J. Subbiah, S. R. Puniredd, B. Purushothaman, W. Pisula, N. Kirby, K. Müllen, D. J. Jones, A. B. Holmes, *J. Mater. Chem.* **2012**, *22*, 21131.
- [149] W. Shin, T. Yasuda, G. Watanabe, Y. S. Yang, C. Adachi, *Chem. Mater.* **2013**, *25*, 2549–2556.
- [150] Z. Jia, Y. Wei, X. Wang, S. Hu, K. Yao, F. Li, *Chem. Phys. Lett.* **2016**, *661*, 119–124.
- [151] J.-L. Wang, Z.-F. Chang, X.-X. Song, K.-K. Liu, L.-M. Jing, *J. Mater. Chem. C* **2015**, *3*, 9849–9858.
- [152] Y. Han, L. Chen, Y. Chen, *J. Polym. Sci. Part A* **2013**, *51*, 258–266.
- [153] Y. Du, Y. Ding, F. Ge, X. Wang, S. Ma, H. Lu, G. Zhang, L. Qiu, *Dyes Pigm.* **2019**, *164*, 27–34.
- [154] P. Edman, L. B.-Å. Johansson, H. Langhals, *J. Phys. Chem.* **1995**, *99*, 8504–8509.
- [155] K. Zhang, P. Wucher, T. Marszalek, M. Babics, A. Ringk, P. W. M. Blom, P. M. Beaujuge, W. Pisula, *Chem. Mater.* **2018**, *30*, 5032–5040.
- [156] X. Wang, X. Miao, L. Ying, W. Deng, Y. Cao, *J. Phys. Chem. C* **2017**, *121*, 19305–19313.
- [157] A. Biadasz, K. Rytel, K. Kędzierski, A. Adamski, M. Kotkowiak, A. Stachowiak, B. Barszcz, H. Y. Jeong, T.-D. Kim, *J. Mol. Liq.* **2019**, *285*, 598–606.
- [158] K. Chung, M. S. Kwon, B. M. Leung, A. G. Wong-Foy, M. S. Kim, J. Kim, S. Takayama, J. Gierschner, A. J. Matzger, J. Kim, *ACS Cent. Sci.* **2015**, *1*, 94–102.
- [159] S. B. Bon, L. Valentini, R. M. Moustafa, F. M. Jradi, B. R. Kaafarani, R. Verdejo, M. A. Lopez-Manchado, J. M. Kenny, *J. Phys. Chem. C* **2010**, *114*, 11252–11257.
- [160] E. Z. Fraczak, T. Makowski, R. M. Moustafa, T. H. El-Assaad, M. E. Moneta, P. Uznanski, B. R. Kaafarani, *J. Mater. Chem. C* **2018**, *6*, 781–789.
- [161] T. Makowski, R. M. Moustafa, P. Uznanski, W. Zajackowski, W. Pisula, A. Tracz, B. R. Kaafarani, *J. Phys. Chem. C* **2014**, *118*, 18736–18745.
- [162] B. Gao, M. Wang, Y. Cheng, L. Wang, X. Jing, F. Wang, *J. Am. Chem. Soc.* **2008**, *130*, 8297–8306.
- [163] B. Wex, A. O. El-Ballouli, A. Vanvooren, U. Zscheschang, H. Klauk, J. A. Krause, J. Cornil, B. R. Kaafarani, *J. Mol. Struct.* **2015**, *1093*, 144–149.
- [164] K. K. McGrath, K. Jang, K. A. Robins, D.-C. Lee, *Chem. Eur. J.* **2009**, *15*, 4070–4077, S4070/1–S4070/5.
- [165] D.-C. Lee, K. Jang, K. K. McGrath, R. Uy, K. A. Robins, D. W. Hatchett, *Chem. Mater.* **2008**, *20*, 3688–3695.
- [166] F. M. Jradi, M. H. Ai-Sayah, B. R. Kaafarani, *Tetrahedron Lett.* **2008**, *49*, 238–242.
- [167] F. S. Raad, A. O. El-Ballouli, R. M. Moustafa, M. H. Al-Sayah, B. R. Kaafarani, *Tetrahedron* **2010**, *66*, 2944–2952.
- [168] B. Kohl, K. Baumgärtner, F. Rominger, M. Mastalerz, *Eur. J. Org. Chem.* **2019**, *2019*, 4891–4896.
- [169] B. Kohl, M. V. Bohnwagner, F. Rominger, H. Wadepohl, A. Dreuw, M. Mastalerz, *Chem. Eur. J.* **2016**, *22*, 646–655.
- [170] B. Kohl, F. Rominger, M. Mastalerz, *Chem. Eur. J.* **2015**, *21*, 17308–17313.
- [171] D.-C. Lee, K. K. McGrath, K. Jang, *Chem. Commun.* **2008**, 3636–3638.
- [172] J. Hu, D. Zhang, S. Jin, S. Z. D. Cheng, F. W. Harris, *Chem. Mater.* **2004**, *16*, 4912–4915.
- [173] S. Leng, L. H. Chan, J. Jing, J. Hu, R. M. Moustafa, R. M. Van Horn, M. J. Graham, B. Sun, M. Zhu, K.-U. Jeong, B. R. Kaafarani, W. Zhang, F. W. Harris, S. Z. D. Cheng, *Soft Matter* **2010**, *6*, 100–112.
- [174] R. M. Moustafa, J. A. Degheili, D. Patra, B. R. Kaafarani, *J. Phys. Chem. A* **2009**, *113*, 1235–1243.
- [175] S. J. Mahoney, M. M. Ahmida, H. Kayal, N. Fox, Y. Shimizu, S. H. Eichhorn, *J. Mater. Chem.* **2009**, *19*, 9221–9232.

Manuscript received: January 14, 2021

Revised manuscript received: February 11, 2021